Chemical Geology 603 (2022) 120880

Contents lists available at ScienceDirect

Chemical Geology

journal homepage: www.elsevier.com/locate/chemgeo

Precipitation sequence of fracture-filling calcite in fractured granite and changes in the fractionation process of rare earth elements and yttrium

Takashi Mizuno [a,*], Antoni Edward Milodowski [b], Teruki Iwatsuki [c]

[a] Geological Disposal Research and Development Department, Japan Atomic Energy Agency, 4-33 Muramatsu, Tokai-Mura, Ibaraki 319-1194, Japan
[b] British Geological Survey (BGS), Keyworth, Nottinghamshire NG12 5GG, UK
[c] Horonobe Underground Research Center, Japan Atomic Energy Agency, Hokushin 432-2, Horonobe-cho, Hokkaido 098-3224, Japan

ARTICLE INFO

Editor: Karen Johannesson

Keywords:
Fracture-filling calcite
Granitic groundwater
Rare earth elements
Uranium

ABSTRACT

This study has focused on the paragenetic sequence, and variation in rare earth elements with yttrium (REY) composition, of fracture-filling calcite in the Toki Granite in the Mizunami area, central Japan. The morphological, chemical, and isotopic characteristics of the calcite and chemistry of fluid inclusions reveal that the calcite in the Toki Granite can be differentiated into four discrete generations: Calcite I (oldest) to Calcite IV (most recent). The precipitation history of calcite reflects the changes in the hydrogeochemical regime of paleo-groundwaters, controlled by the evolution of groundwater by seawater infiltration associated with marine transgression and surface water infiltration associated with marine regression and uplift. The post-Archean average shale-normalized REY patterns in each generation of calcite show no significant Ce anomaly, negative Eu anomaly, and a light REY (LREY)-depleted pattern dominates. These features are also common to the Toki Granite. The consistency of the features in each generation of calcite indicates that REY was supplied from the Toki Granite by water-rock interaction. The lack of a Ce anomaly in the calcite demonstrates that groundwaters have maintained reducing conditions during the calcite precipitation. However, the fractionation of LREY and heavy REY in each generation of the calcite is more pronounced than in the granite. The fractionation process in the paleo-groundwaters from which each generation of calcite precipitated closely relates to the systematic variation of carbonate complex in the REY series and/or pH in palaeo-groundwater. The findings of this study will be important for assessing the long-term safety of geological disposal of high-level radioactive waste.

1. Introduction

Understanding the potential migration behavior of radioactive species in the deep sub-surface is essential in evaluating the long-term post-closure safety (over timescales of tens of thousands to hundreds of thousands of years) of a geological disposal system for high-level radioactive waste (HLRW) (OECD/NEA, 2012; OECD NEA, 2013). However, there is uncertainty in the reliability of modeling radionuclide migration over such long periods, based solely on extrapolation of data from "short-term" laboratory or in situ field experiments (which are typical of the order of only months to tens of years). Confidence in long-term model predictions can be enhanced by checking against observations from natural geological systems ("natural analogues"), where processes relevant to radioactive waste disposal have operated over comparably long timescales (i.e., thousands to millions of years).

Rare earth elements (REE), particularly light REE, can be studied as analogues of certain trivalent actinides (e.g., Am^{3+}, Cm^{3+}, Cf^{3+}, and Pu^{3+}) in the natural environment because of their identical valence and similar ionic radii (Johannesson and Hendry, 2000; Stipp et al., 2006; Wood, 1990), as well as representing analogues for REE fission products (e.g., Ce-144, Pm-147 and Eu-154) (Miekeley et al., 1992). Yttrium also forms a trivalent cation that exhibits similar geochemical behavior and is commonly discussed along with the REE (Mathurin et al., 2014; Möller and De Lucia, 2020; Qin et al., 2020). Therefore, observations on the REE and yttrium (REY) distribution between groundwater and associated secondary mineral precipitates may provide useful analogue insights into the long-term migration and retardation of actinide species in the geological environment.

The use of hydrological techniques and hydrochemical data to evaluate the long-term paleohydrogeological evolution of groundwater systems is limited by the transient nature of groundwater. Past groundwaters will tend to be flushed, for example, by steady-state flow

* Corresponding author.
E-mail address: mizuno.takashi@jaea.go.jp (T. Mizuno).

https://doi.org/10.1016/j.chemgeo.2022.120880
Received 13 January 2022; Received in revised form 31 March 2022; Accepted 20 April 2022
Available online 27 April 2022

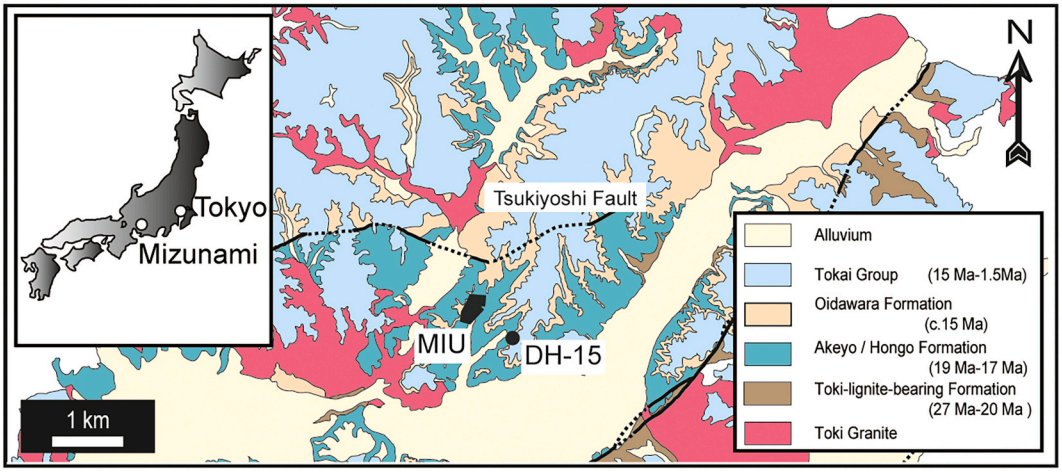

Fig. 1. Geological map of the Mizunami area and locations of the DH-15 borehole and the Mizunami Underground Research Laboratory (MIU).

and mixed with or replaced by later groundwater of different origins that may be recharged under different conditions associated with changes in uplift, marine transgression, and regression. Consequently, the geochemical signature of the earlier groundwater may be lost completely, or the mixing of different groundwaters may complicate its interpretation, or it may reflect conditions elsewhere along the flow path (Metcalfe et al., 1998). In contrast, minerals precipitated from groundwater are much less easily removed by subsequent groundwater flushing events. Consequently, their textural or geochemical features can better preserve a record of groundwater history, both at a specific location and over a much longer period (Metcalfe et al., 1998; Milodowski et al., 1998). Low-temperature or contemporary calcite mineralization is commonly closely associated with fracture-controlled active deep groundwater systems at many radioactive waste disposal research sites in crystalline rocks in Japan, Europe, USA, and Canada (e.g., Blyth et al., 2009; Drake and Tullborg, 2009; Iwatsuki et al., 2002; Milodowski et al., 2015, 2018; Sandström and Tullborg, 2009; Tullborg and Drake, 2008) and can potentially preserve information on the chemical composition (Metcalfe et al., 1998; Milodowski et al., 1998); redox conditions (Barnaby and Rimstidt, 1989; Frank et al., 1982; Franklyn et al., 1991; Milodowski et al., 2018), temperature (Iwatsuki et al., 2002; O'Neil et al., 1969), and age (Roberts et al., 2020) of the paleo-groundwater from which calcite precipitated. Furthermore, REY is strongly partitioned into calcite during precipitation (Möller and De Lucia, 2020; Tanaka and Kawabe, 2006; Terakado and Masuda, 1988; Toyama and Terakado, 2014; Voigt et al., 2017; Zhong and Mucci, 1995). Therefore, by combining information on REY abundances and the chemical conditions preserved in calcite, we can understand the variations in REY abundance and their behavior in paleo-groundwaters.

The Japan Atomic Energy Agency (JAEA) has been conducting research and technique development for the geological disposal of HLRW. The research program includes the development of the Mizunami Underground Research Laboratory (MIU) in the central part of Japan, which is a generic underground research laboratory (URL) located within the Cretaceous Toki Granite (JAEA, 2011, 2016; JNC, 2000). Previous studies have shown that the REY signature of the deep groundwater in the Mizunami area is derived from the granite by rock-water interaction (Takahashi et al., 2002), and in turn, REY distribution in the secondary fracture-filling minerals (including calcite) reflects that of the groundwater (Munemoto et al., 2015; Wogelius et al., 2020). This study focused on the minor (Mg, Mn, and Fe) and trace (REY and U) elements in the fracture-filling calcite in the Toki Granite to examine their long-term migration behavior in response to changes in hydrogeological and hydrochemical conditions.

2. Study site

The Mizunami area is located approximately 40 km northeast of Nagoya. The basement bedrock is the Cretaceous Toki Granite (Fig. 1). The Mizunami Group and the Seto Group, comprising Tertiary and Quaternary sedimentary rocks, were unconformably deposited on an eroded Toki Granite surface (Sasao, 2013) (Fig. 1). The depositional environment of the Mizunami Group changed over time. In its early stages, fluvio-lacustrine arenaceous and conglomeratic sediments of the Toki Lignite-bearing Formation (~27–20 Ma) were deposited (Hiroki and Matsumoto, 1999; Sasao et al., 2006), The Toki Lignite-bearing Formation is rich in organic matter, and the Tono Uranium Deposit is hosted in this formation (Sakamaki, 1985). This was followed by marine transgression resulting in the deposition of a ~ 200 m thick sequence of shallow water marine tuffaceous sandstones and siltstones comprising: the Hongo and Akeyo Formations (19–17 Ma), interrupted by a period of regression, erosion, and non-deposition (17–15 Ma), before renewed deposition of the Oidawara Formations (15 Ma) (Sasao et al., 2006). The potential provenance of the volcanic ash has not yet been identified (Sasao, 2013). Subsequently, the lacustrine Tokai Group was deposited between 12 and 1.5 Ma (Sasao et al., 2006).

In the Mizunami area, the present-day groundwater is dominated by Na–Ca–HCO_3-type groundwater. However, Na–Cl-type groundwater occurs in the discharge area of the groundwater flow system on a regional scale of ~100 km^2 centered on the MIU (Iwatsuki et al., 2010; Iwatsuki and Yoshida, 1999; Metcalfe et al., 2003). Both groundwaters have a weakly alkaline pH (Iwatsuki et al., 2005; Iwatsuki and Yoshida, 1999). The analyses of the stable oxygen and hydrogen isotopic compositions of the groundwaters show that meteoric water is their primary origin in this region (Iwatsuki et al., 2005; Iwatsuki and Yoshida, 1999; Munemoto et al., 2015). However, Iwatsuki et al. (2002) demonstrated that groundwaters of hydrothermal, meteoric, and seawater origin all existed in the past in the Mizunami area. Furthermore, Mizuno et al. (2010) differentiated four stages in calcite mineralization that represent the latest stages of the regional mineralization paragenesis. Calcite veins cross-cut, and post-date, early high-temperature hydrothermal vein mineralization dominated by silicate minerals (principally quartz, K-feldspar, albite, chlorite, epidote, and sericite), with minor fluorite and accessory sulfide minerals (pyrite, sphalerite, chalcopyrite, galena), and hematite (Milodowski et al., 2005). Based on their petrographic relationships, crystal morphology, compositional growth zoning characteristics, and isotopic composition, these four generations of calcite are defined as Calcite I, Calcite II, Calcite III, and Calcite IV (from oldest to youngest). This sequence of calcite mineralization has previously been interpreted to potentially reflect the changes in origin of the

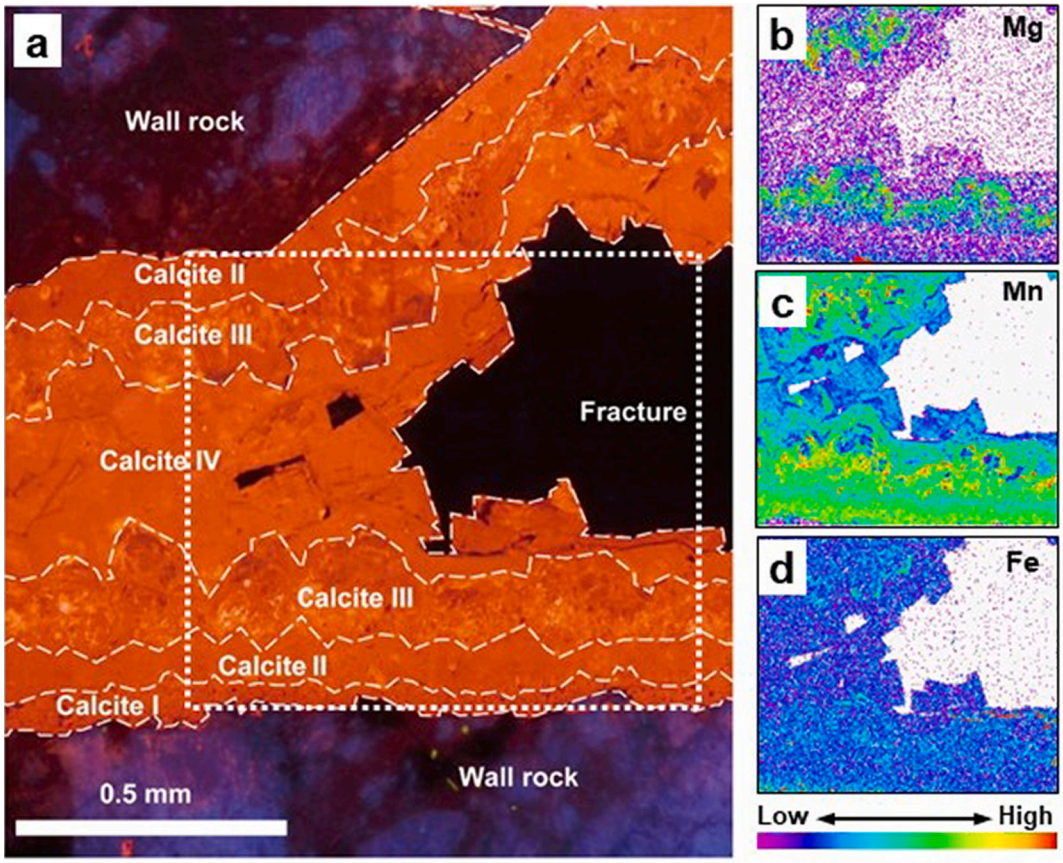

Fig. 2. (a) Cathodoluminescence image of the fracture-filling calcite demonstrating a precipitation sequence that can be divided into four generations in the sample taken from the DH-15 borehole at a depth of 913.0 m. Chemical mapping of (b) Mg, (c) Mn, and (d) Fe was produced by EPMA from the area shown on the CL image by the dotted outline.

groundwater from which each generation of calcite precipitated - from hydrothermal fluid, to freshwater, to seawater, and finally freshwater again - following the emplacement of the Toki granite to the deposition of the Tokai Group (Iwatsuki et al., 2002; Mizuno et al., 2010).

The chondrite-normalized REY pattern in the present-day granitic groundwater demonstrates a light REY (LREY) enrichment and a negative Eu anomaly, similar to that of the Toki granite (Takahashi et al., 2002). However, in the shallow groundwater zone (depth down to 400 m) around the MIU, the penetration of surface groundwater accompanying the excavation of the shaft promoted the sorption of REY (particularly LREY) into the bedrock. Consequently, the shallow groundwater exhibits a more heavy REY (HREY)-rich pattern than the deep groundwater (Munemoto et al., 2015). Below 500 m, the influence of surface groundwater invasion is negligible, and the deep groundwater preserves the same LREY enriched pattern as that of the granite host rock. The overall change in REY abundance from deep to shallow groundwater generally corresponds with changes in REY abundance from old to young groundwater (Munemoto et al., 2015).

3. Materials and methods

In this study, the calcite samples were obtained from the DH-15 borehole drilled in the southeastern part of the Mizunami area, which is located in the regional groundwater flow system (Fig. 1). DH-15 is a vertical borehole that was cored to a depth of ~1000 m. For this study, the fracture-filling calcite in the Toki Granite was sampled from ten open fractures lined with euhedral crystals of sufficient size (~1 mm or greater) to enable detailed petrographic observation and analysis. These open fractures were closely associated with known intervals of groundwater inflow in the borehole, and therefore considered to be potentially conductive or flowing features, based on hydraulic packer tests and/or flowmeter logging (Takeuchi et al., 2013).

Detailed petrographic analysis was carried out by optical microscopy, cathodoluminescence microscopy (CL), and scanning electron microscope (SEM). SEM analysis was carried out using a LEO 435VP variable-pressure digital SEM equipped with an Oxford Instruments INCA energy-dispersive X-ray microanalysis (EDXA) system. The calcite crystals were initially observed in the SEM as uncoated samples under low-vacuum mode using backscattered electron (BSE) imaging to characterize their crystal morphology. Subsequently, polished thin sections were prepared for more detailed optical petrography and BSE-EDXA observation and analysis. The polished thin sections were also observed for CL imaging using a Technosyn 8200 (Mk II) cold-cathode stage mounted on a Nikon optical microscope. The vacuum, beam voltage, and current settings were adjusted, as required, to generate optimum luminescence. Based on the CL images, selected areas were microchemically-mapped by wavelength-dispersive electron probe microanalysis (EPMA) to examine the distribution of Mg, Fe, and Mn. These maps were produced using a Cameca SX50 electron microprobe and generated at 15 kV, and 100 nA, typically with a spot size of 2 μm (diameter) and a pixel dwell time of 90 ms. From the CL images and the elemental mapping results, the compositional growth-zoning structure within the calcite crystals was clearly defined.

Quantitative analysis of Mg, Mn, Fe, REY, and U was undertaken directly on the calcites observed in polished thin sections, using laser ablation microprobe - inductively coupled-plasma mass spectrometry (LAMP-ICP-MS). The analytical system used a Spectron Nd YAG ultraviolet laser, a 266-nm-sized wavelength linked to a high-quality Leitz optical microscope. An Ar carrier gas stream then transfers the ablated material from the ablation chamber to the plasma source in a VG

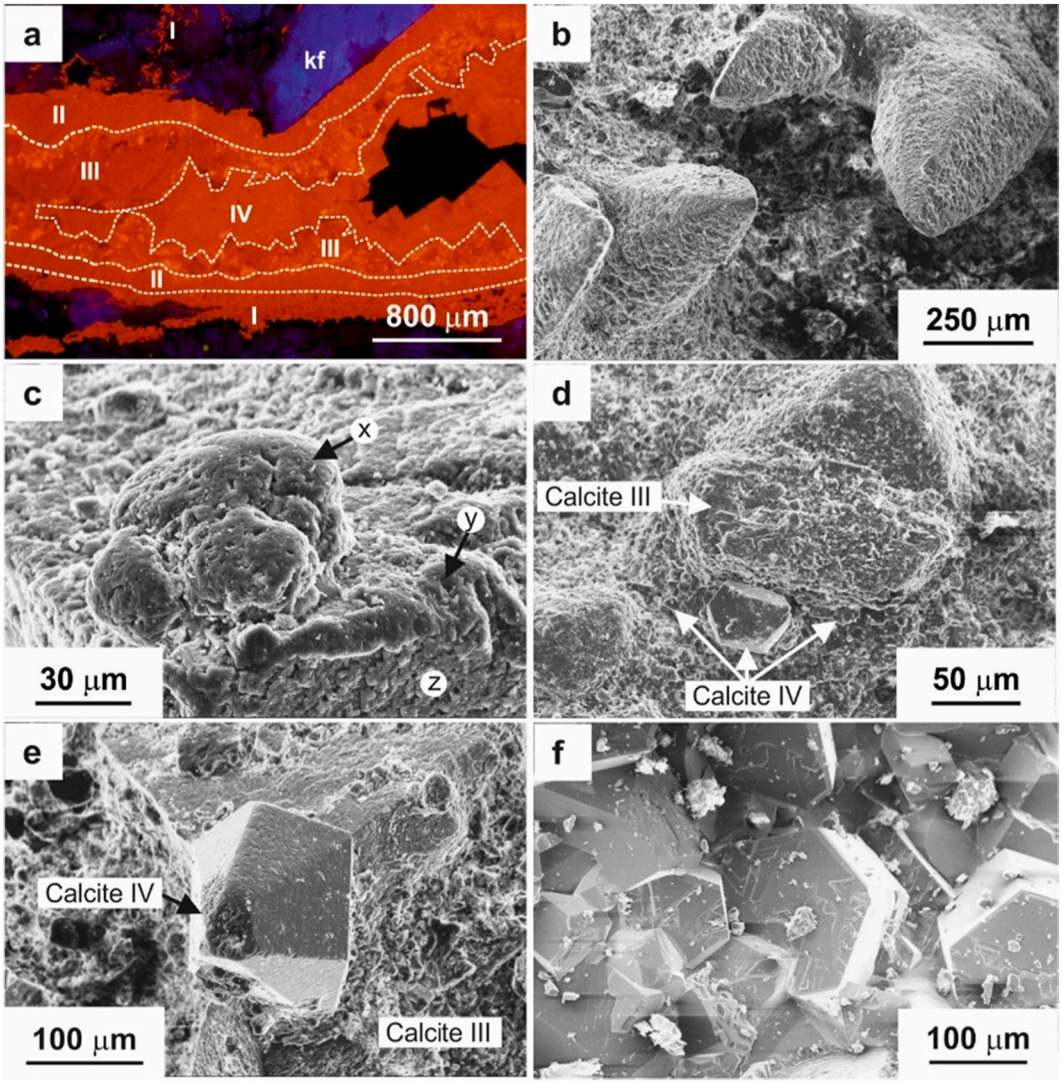

Fig. 3. CL and SEM images illustrating the petrographic and morphological characteristics of late-stage fracture-filling calcite from borehole DH-15: (a) CL image of complex multi-generational calcite vein (913.0 m depth) containing Calcite I, II, III, and IV. Anhedral Calcite I mineralization lining the fracture wall contains fine, non-luminescent inclusions of comminuted wall rock, fills microfractures penetrating the adjacent wall rock, and partially replaces wall rock minerals such as non-luminescent plagioclase and blue-luminescent K-feldspar (kf); (b) SEM image of euhedral Calcite III (427.3 m depth) demonstrating its characteristic c-axis elongated crystal form, showing etched and pitted crystal surfaces coated with a microcrystalline precipitate of later Calcite IV; (c) SEM image of micro-colloform or "globular" precipitates of Calcite IV (x) nucleated on the corroded crystal faces (z) and edges (y) of euhedral Calcite III (427.3 m depth); (d) SEM image showing the early stages in the development of euhedral Calcite IV overgrowths on strongly corroded surfaces of Calcite III; (e) SEM image of a well-developed euhedral c-axis flattened Calcite IV syntaxial overgrowth nucleated on a corroded Calcite III (427.3 m depth); (f) Well-developed euhedral crystals of Calcite IV (996.2 m depth) showing typical c-axis flattened tabular and equant crystal forms. (For interpretation of the references to colour in this figure legend, the reader is referred to the web version of this article.)

Table 1
The sampling depths of the fracture-filling calcite in the Toki Granite and the observed distribution of different generations of calcite in each sample.

Sampling depth of fracture-filling calcite	Observed Generation			
(GL-m)	I	II	III	IV
238.7	Yes	Yes	Yes	No
303.1	Yes	Yes	No	Yes
427.3	Yes	Yes	Yes	Yes
442.5	No	Yes	Yes	Yes
475.5	Yes	Yes	Yes	Yes
573.0	Yes	Yes	Yes	No
913.0	Yes	Yes	Yes	Yes
930.2	Yes	No	No	No
995.2	Yes	Yes	Yes	Yes
996.2	No	Yes	No	Yes

Plasmaquad 2+ spectrometer ICP-MS instrument using a modified dual-flow sample introduction system. The analytical procedure followed Chenery and Cook (1993); with NIST SRM 613 glass used as calibration reference material. Analytical precision and accuracy were checked against BHVO-2G glass as an independent standard and calculated on the basis of six replicate analyses. Analytical values for REY were within 15% of the standard value. Full details of the detection limits, precision, and accuracy of each measured element are given in Table S1. Because of the difference in ablation efficiency between the standard reference material and the calcite samples, in this study, the LAMP-ICP-MS analysis data were normalized to ^{44}Ca, which was then scaled to an "idealized" calcite composition stoichiometry (i.e., assuming a nominal Ca ≡ 400,000 mg/kg for pure $CaCO_3$). In reality, this overestimates the trace element concentration since these calcites are mildly magnesian and ferromanganoan, and therefore the actual Ca concentration will be lower than for pure $CaCO_3$. However, for most analyses, the total

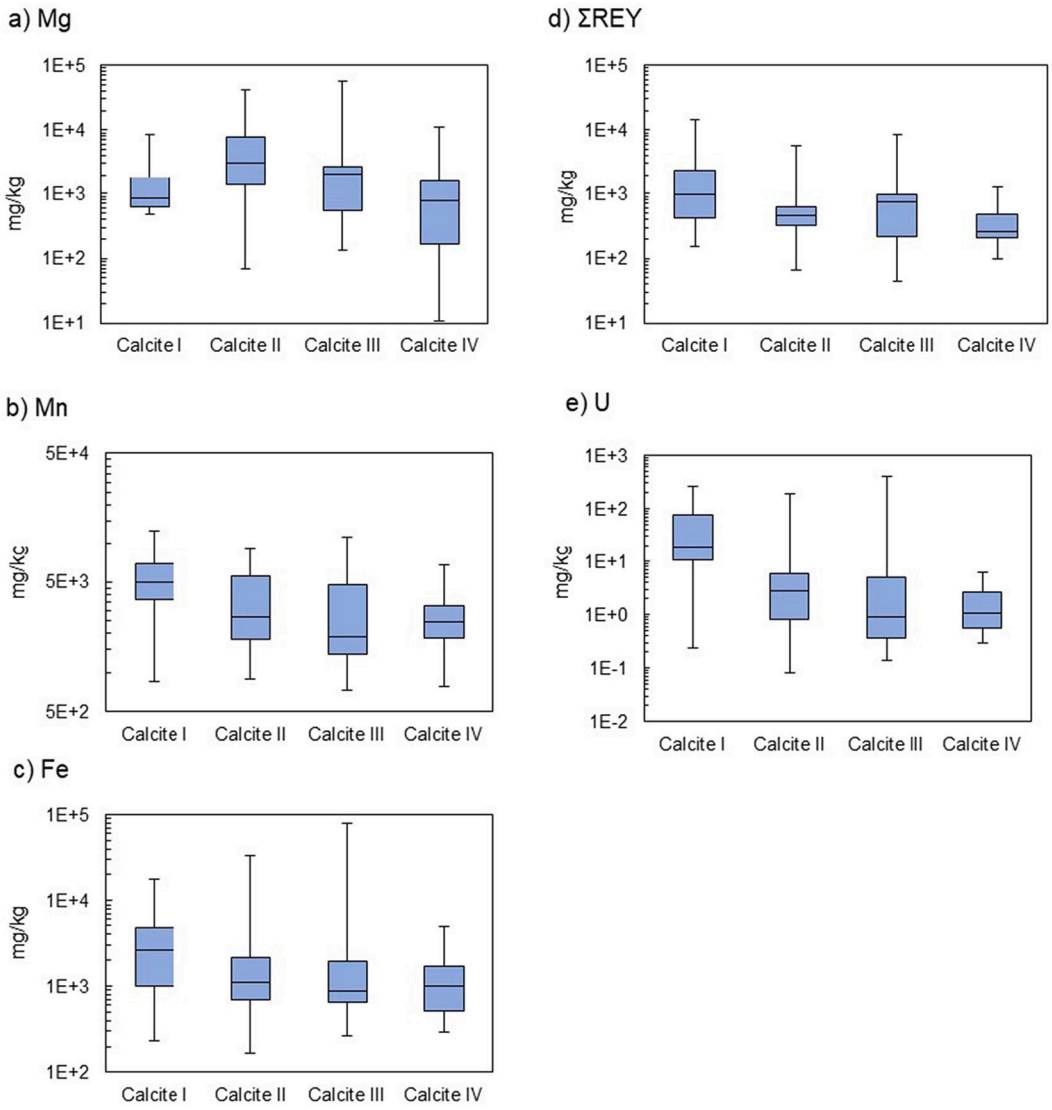

Fig. 4. The box plots with maximum and minimum values of (a) Mg, (b) Mn, (c) Fe, (d) ΣREY, and (e) uranium in each generation of fracture-filling calcite.

amount of Fe, Mn, and Mg is less than 5% of the mass of Ca. Consequently, any overestimation of trace element concentration is relatively small (i.e., less than the analytical error). Furthermore, this does not impact the overall pattern of post-Archean average shale (PAAS)-normalized distribution plots of Y and REE derived from these calcite data. Therefore, this simplified approach is considered to be appropriate for comparative purposes in this study.

4. Results

4.1. Macroscopic and microscopic observations

The CL and SEM observations show that four generations of calcite mineralization can be differentiated, referred to (from oldest to youngest) as Calcite I to IV (Fig. 2, Fig. 3a; Table 1). The relative concentration distribution of the metal elements, as indicated by EPMA mapping, is also helpful in distinguishing the calcite generations. (Fig. 3b, c, and d). All the samples display textural evidence of repeated fracture reactivation, involving movement with brecciation, dilation, and subsequent overgrowth of one or more generations of later calcite mineralization on earlier calcite mineralization (e.g., Fig. 2). No localized concentration or relationship to depth was observed in the distribution of each generation of calcite. The characteristics of calcite for each generation are listed below.

Calcite I: This is the earliest precipitated calcite with moderate to bright luminescence. It commonly contains a considerable amount of included comminuted wall rock fragments and may mineralize some earlier hydrothermal veins, which have been reactivated by later movement. The calcite may locally replace primary granite minerals (principally plagioclase and biotite) and fill microfractures in the immediately adjacent host rock (Fig. 3a). In some cases, Calcite I was immediately preceded by the localized injection of light gray, finely-comminuted, and argillised (smectitic) granitic material into dilatant fractures as fluidized fine sand- to silt-grade sediment (i.e., "cataclastic injectite"). This was subsequently partially replaced and tightly cemented by microcrystalline Calcite I (e.g., the sample from 930.2 m, Table 1). Calcite I is typically anhedral. Qualitative EPMA elemental mapping shows that this generation of calcite has relatively high Mn and Fe concentrations and a very low concentration of Mg (Fig. 2b-d).

Calcite II: This was precipitated on top of an irregular substrate of Calcite I. It displays moderate to bright luminescence, similar to that of Calcite I (Fig. 2a, Fig. 3a), but in contrast, it is devoid of inclusions of comminuted rock fragments. Multiple samples show Calcite II is subsequently enclosed beneath later Calcite III and IV. The external crystal form of Calcite II cannot be directly observed because it is obscured by extensive syntaxial overgrowths of Calcite III, which dominate the

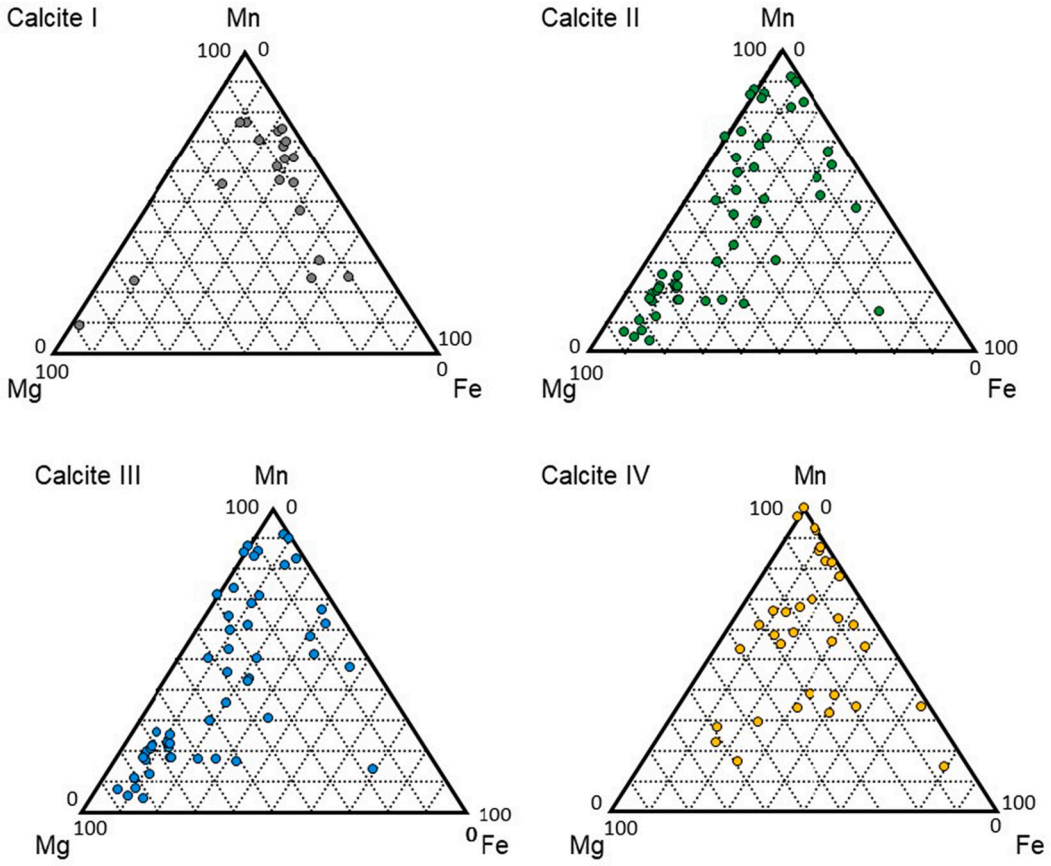

Fig. 5. The ternary plots based on Mg, Mn, and Fe concentration in each calcite generation.

external crystal morphology of the calcite mineralization. However, the growth zoning characteristics revealed under CL suggest that the Calcite II (which forms the cores of these composite calcite crystals) tended to develop as equant to slightly *c*-axis elongated crystals. This contrasts to the markedly *c*-axis elongated growth forms exhibited by the subsequent syntaxial overgrowths of Calcite III. Qualitative EPMA elemental mapping (Fig. 2b-d) shows that this calcite is broadly similar in composition to Calcite I.

Calcite III: This was typically precipitated as syntaxial overgrowths that nucleated on top of Calcite II. It demonstrates locally and variably bright luminescence, although the overall luminescence is generally duller than Calcite I, II, and IV. The crystals of this generation are distinctly elongated along the *c*-axis (Fig. 3b). These commonly display etching of their surfaces prior to overgrowth or encrustation by later Calcite IV (Fig. 3b-d). Qualitative EPMA element maps show that Mn and Fe concentrations are relatively low, but the Mg concentrations are relatively high in comparison to Calcite I and II (Fig. 2b-d). The corrosion and etching of Calcite III surfaces clearly indicate a hiatus in calcite mineralization that was associated with a period of minor calcite dissolution, followed by the renewal of calcite mineralization resulting in the precipitation of Calcite IV.

Calcite IV: This is the youngest generation of calcite observed and rests on earlier calcite substrates (Fig. 2a, Fig. 3a). It displays relatively bright luminescence, broadly similar to those of Calcite II. Calcite IV is commonly seen as microporous or gel-like "globular" deposits or microcrystalline coatings on the corroded surfaces of euhedral crystals of Calcite III (Fig. 3c). However, as Calcite IV became more extensively developed, this poorly-crystalline calcite was progressively overprinted or replaced by well-formed euhedral overgrowths (Fig. 3d, e) or by clusters of euhedral crystals lining open fracture cavity walls (Fig. 3f). Typically, the well-developed Calcite IV crystals display euhedral c-axis flattened tabular to more equant rhombohedral crystal forms (Fig. 3e, f). Qualitative EPMA element maps indicate that this generation of calcite is slightly lower in Fe and Mn than in Calcite I and Calcite II.

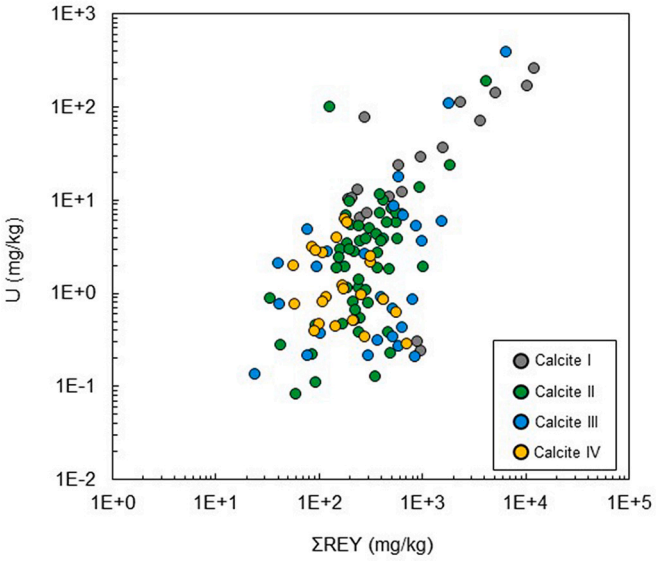

Fig. 6. Relationship between ΣREY and uranium concentration (r = 0.85 in all samples).

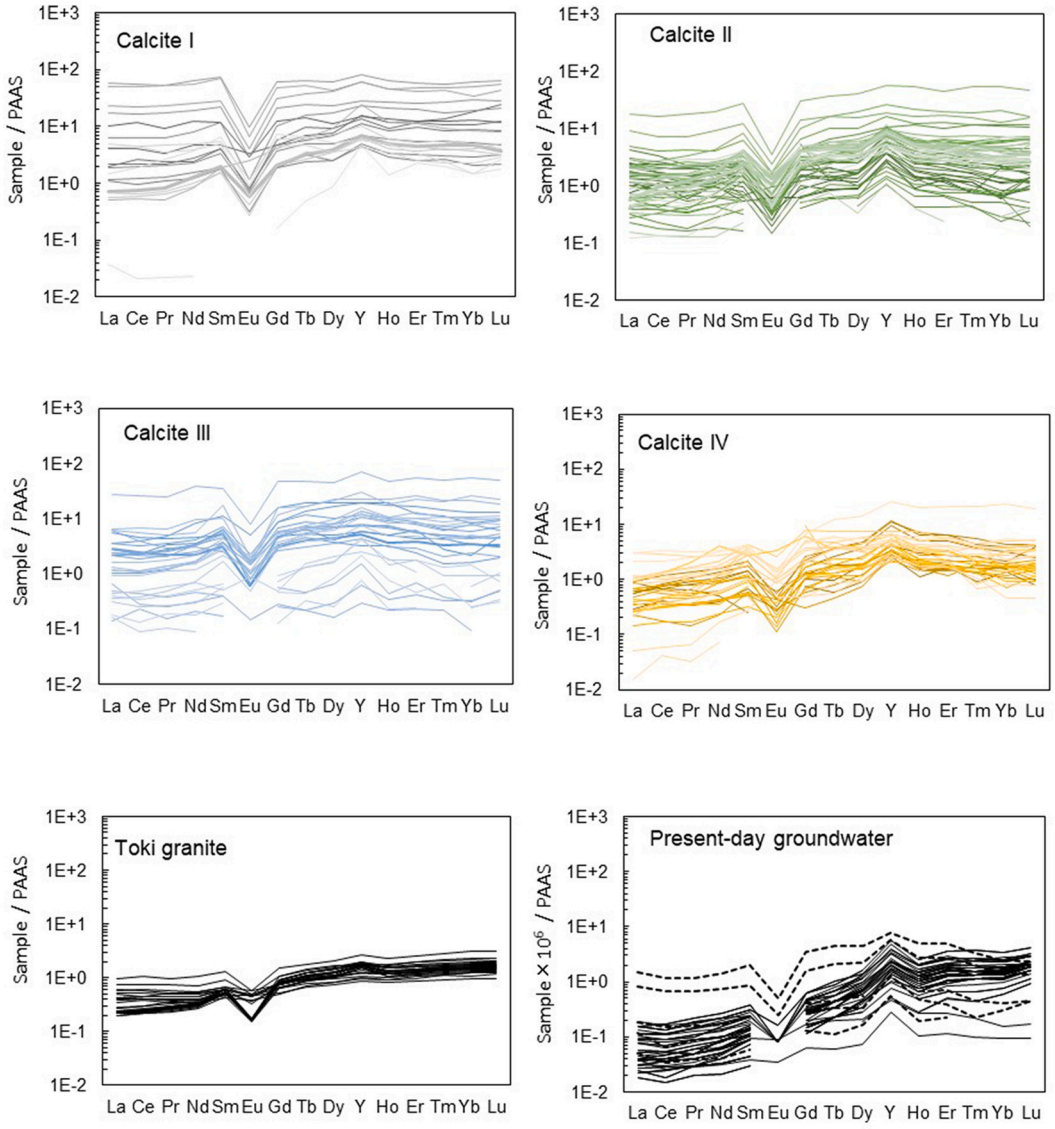

Fig. 7. PAAS-normalized REY patterns for each generation of calcite, the Toki granite, and present-day groundwater. Those for the Toki granite were from Takahashi et al. (2002), Yamamoto et al. (2013), and Wogelius et al. (2020), and for present-day groundwater are from Takahashi et al. (2002), Munemoto et al. (2015), and Iwatsuki et al. (2017). For the groundwaters, the solid lines represent the REY patterns of present-day shallow groundwater (<500 m depth), and the broken lines represent groundwaters sampled from deep underground (>500 m depth).

4.2. Minor (Mg, Mn, and Fe) and trace (REY and U) elements in the fracture-filling calcite

All generations of calcite exhibit a wide range of minor (Mg, Mn, and Fe) and trace (REY and U) element concentrations (Fig. 4; Table S2, S3). The statistical differences between each generation of these elements are confirmed based on the non-parametric Mann–Whitney *U* test. As a result, Calcite I shows significantly higher Mn, Fe, total REY (ΣREY), and U concentrations, except for ΣREY and Fe concentrations to Calcite III (Fig. 4; Table S3). Calcite II and Calcite III shows significantly higher Mg concentration than Calcite IV (Fig. 4a; Table S3). Calcite IV shows significantly lower ΣREY. Ternary plots of Mg, Mn, and Fe indicate that Calcite I is relatively depleted in Mg, Calcite II and Calcite III show a similar relative enrichment in Mg and are depleted in Fe. Calcite IV has no distinctive tendencies (Fig. 5). ΣREY and U concentration in each generation show a positive correlation except for Calcite IV ($r = 0.94$ in Calcite I; $r = 0.82$ in Calcite II; $r = 0.96$ in Calcite III; $r = -0.23$ in Calcite IV), although overall there is a good positive correlation across the all generations ($r = 0.81$) (Fig. 6).

Post-Archean average shale (PAAS)-normalized (Pourmand et al., 2012) REY distribution patterns comparing the fracture filling calcites, Toki Granite, and present-day groundwaters are shown in Fig. 7, with key REY ratios summarizing the shape of these profiles and associated REY anomalies are presented in Table 2. The PAAS-normalized REY distribution patterns for the Toki granite, groundwaters, and fracture-filling calcites all display a marked negative Eu anomaly. Calcites I, II, and III have broadly similar PAAS-normalized REY distribution patterns, although, in general, the absolute REY concentrations may be up to an order of magnitude higher for Calcite I (Table S3). Fig. 7 illustrates that these calcites are displayed between 1 and 2 orders of magnitude enhancement in REY compared to the host Toki Granite. In addition, Calcite I, II, and III are generally more enriched in the LREY relative to the HREY, although deeper groundwaters (>500 m depth) also display similar relative enrichment in LREY against HREY. No statistical difference was found between La_{SN}/Yb_{SN} values in Calcite I, Calcite II, and Calcite III (non-parametric Mann–Whitney U test). In contrast, the shape of the REY distribution profile for Calcite IV more closely matches that of the present-day shallow groundwaters (<500 m depth), but with

Table 2
Key indicator REY ratios summarizing the profile and anomalies PAAS-normalized REY distribution patterns of each generation of calcite, Toki granite, shallow and deep groundwater. REY_{SN} means shale (PAAS) normalized value of REY. Ce_{SN} * and Eu_{SN}* are $0.5La_{SN} + 0.5Pr_{SN}$, $0.5Sm_{SN} + 0.5Gd_{SN}$, respectively.

		Ce_{SN}/Ce_{SN}*	Eu_{SN}/Eu_{SN}*	La_{SN}/Yb_{SN}	La_{SN}/Gb_{SN}	Gd_{SN}/Yb_{SN}	Y_{SN}/Ho_{SN}
Calcite I	Maximum	1.2	0.85	2.2	1.1	5.1	3.4
	Median	0.98	0.17	0.39	0.60	0.64	1.4
	Minimum	0.71	0.10	0.03	0.13	0.11	1.0
Calcite II	Maximum	1.6	1.09	3.2	2.5	3.9	3.1
	Median	0.97	0.24	0.43	0.52	0.93	1.7
	Minimum	0.65	0.11	0.02	0.10	0.11	0.88
Calcite III	Maximum	1.5	1.8	2.7	2.3	2.7	3.4
	Median	0.90	0.28	0.49	0.42	0.87	1.37
	Minimum	0.61	0.11	0.04	0.12	0.37	0.97
Calcite IV	Maximum	1.7	2.5	1.3	1.2	5.5	2.3
	Median	1.02	0.33	0.24	0.31	0.83	1.7
	Minimum	0.85	0.09	0.03	0.02	0.21	0.75
Toki granite	Maximum	1.1	0.94	0.41	0.80	0.58	1.5
	Median	1.00	0.28	0.17	0.34	0.50	1.20
	Minimum	0.9	0.19	0.11	0.24	0.40	1.0
Shallow Groundwater	Maximum	1.1	0.35	0.59	0.58	1.1	2.9
	Median	0.89	0.24	0.04	0.22	0.18	1.8
	Minimum	0.62	0.17	0.01	0.11	0.10	1.4
Deep Groundwater	Maximum	0.87	0.20	0.59	0.53	1.4	2.1
	Median	0.86	0.19	0.58	0.47	1.3	1.8
	Minimum	0.86	0.18	0.58	0.42	1.1	1.6

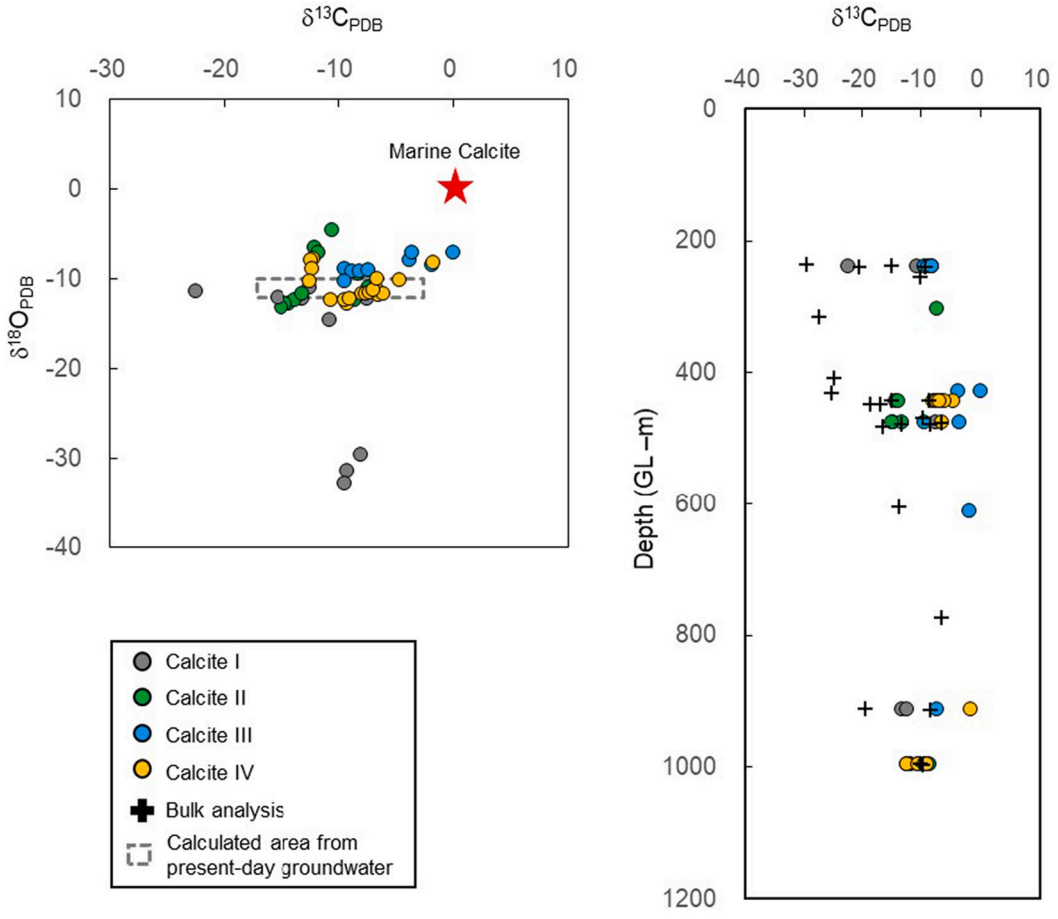

Fig. 8. Isotopic characteristics of fracture-filling calcite in DH-15 borehole. The isotope data were obtained from different calcite crystals to those analyzed for REY in this study. (a) Cross-plot of the variation in $d^{13}C_{PDB}$ vs $d^{18}O_{PDB}$ for each calcite generation. The dashed outline box shows the range of $d^{13}C_{PDB}$ and $d^{18}O_{PDB}$ in calcite calculated to be in equilibrium with the present-day groundwaters using carbon (Emrich et al., 1970) and oxygen (O'Neil et al., 1969)isotopic equilibrium constant between calcite and fluid. (b) Plot showing the variation in $d^{13}C_{PDB}$ with depth for fracture-filling calcite in the DH-15 borehole. Data source: Mizuno et al. (2010) for calcite; Iwatsuki et al. (2005) and Suzuki et al. (2014) for groundwaters.

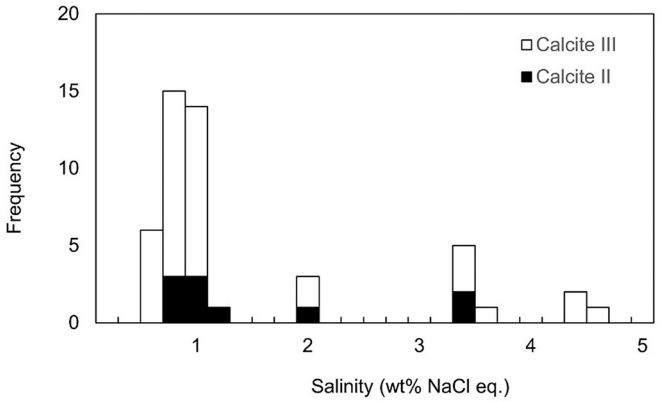

Fig. 9. Salinity of fluid inclusions in Calcite II and Calcite III. Data source: Mizuno et al. (2010).

absolute concentration enhanced by about 1 order of magnitude. This generation of calcite is significantly less enriched in LREY compared to Calcite I, Calcite II, and Calcite III, which is more similar to the host granite. A key feature of the PAAS-normalized REY distribution patterns in both the groundwaters and most of the fracture calcites (particularly Calcite II, III and IV) is the presence of a positive Y anomaly. This is absent in the Toki Granite.

5. Discussion

5.1. Precipitation history of calcite

The paragenetic sequence of four distinct generations of late-stage calcite fracture mineralization identified in this study agrees with the results of previous studies (Iwatsuki et al., 2002; Mizuno et al., 2010). Detailed petrographic analyses from this study, together with fluid inclusion microthermometry and stable (C, O) isotope data of fracture-filling calcite obtained from the same borehole during the earlier studies, potentially enable the mineralization to be correlated with the geological evolution of the Mizunami area.

Calcite I has a strongly depleted ^{18}O signature ($\delta^{18}O_{PDB}$ mainly lighter than −20‰) (Fig. 8a). Since the distribution coefficient of oxygen isotopes between groundwater and calcite is temperature dependent, it is possible to estimate the temperature when the calcite precipitated (O'Neil et al., 1969). In fact, the lighter $\delta^{18}O_{PDB}$ in Calcite I is far different from the isotopic composition in the calcite precipitated from present-day groundwater or seawater (Fig. 8a). The lightest $\delta^{18}O_{PDB}$ in Calcite I (−32.7‰) indicates it was probably deposited from a warm hydrothermal fluid (at least 90 °C) (Iwatsuki et al., 2002). Previous studies have also shown that calcite was precipitated in high-temperature environments during the late-stage cooling of the Toki Granite (Ishibashi et al., 2016). Based on apatite fission-track ages, the temperature of the Toki Granite is estimated to have cooled to between 90 °C to 120 °C at 37.6–39.8 Ma (Yamasaki and Umeda, 2012), and hydrothermal events have not been identified after that time (Sasao et al., 2006). Therefore, Calcite I is considered to have formed during this period.

The later generations of fracture-filling calcite commonly display euhedral crystal morphologies, and their crystal forms change through each generation. The morphology of calcite crystals may reflect the groundwater composition from which the calcite precipitated. For example, previous studies have shown that calcite with crystals elongated along the *c*-axis may form in brackish to saline, and Mg-rich environments, whereas *c*-axis flattened and rhombohedral crystals tend to precipitate from more dilute (fresh) groundwater (Davis et al., 2004; Folk, 1974; Lahann, 1978; Milodowski et al., 2005, 2018; Sakamaki, 1985). Calcite growth morphology can also be influenced by other chemical components (e.g., organics, SO_4, Mn^{2+}, and Sr^{2+} (Astilleros et al., 2002; Kimbell and Humphrey, 1994; Parker et al., 1993; Temmam et al., 2000), and by the degree of saturation, temperature, or fluid flow rates (Given and Wilkinson, 1985; Gonzalez et al., 1992).

Assuming the relationship between salinity and calcite crystal morphology observed in other studies also holds true for the Mizunami mineralization, Calcite III (which develops *c*-axis elongated crystals) is interpreted here to have precipitated from a brackish to saline groundwater. This is supported by microthermometric analysis of fluid inclusions from Calcite III (Milodowski et al., 2005; Mizuno et al., 2010), which clearly demonstrated the mineralizing fluid had a salinity ranging between 0.47 and 4.53 wt% equivalent NaCl (Fig. 9). The crystal growth morphology of Calcite II is not well defined, but fluid inclusion analyses show that it also precipitated from a fluid with a similar salinity (0.47 to 3.26 wt% equivalent NaCl) (Fig. 9). The fluid inclusions in both Calcite II and Calcite III are all monophase, which indicates they both formed below 80 °C (Roedder, 1984), consistent with their stable isotope composition ($\delta^{18}O_{PDB}$ typically between −7 to −12‰), which is much less depleted in ^{18}O than Calcite I (Fig. 8a) and implies mineralization under cooler conditions. No fluid inclusion data could be obtained from Calcite IV (Milodowski et al., 2005; Mizuno et al., 2010), but the similarity in its $\delta^{18}O_{PDB}$ values (Fig. 8a) suggests that the formation temperature was possibly similar to Calcite II and Calcite III.

The period when seawater intrusion may have influenced the groundwater system was potentially from the beginning of the deposition of the Hongo Formation, a shallow marine deposit, at 19 Ma to the end of the deposition of the Oidawara Formation associated with a major seaward movement event at 15 Ma. It may be assumed that meteoric water infiltrated the area during the period of the unconformity between the Akeyo and Oidawara Formations from 17 to 15 Ma. However, since the uplift of this area had not begun at that time, the hydraulic gradient was small, and it can be assumed that the groundwater originated from seawater was retained. The salinity comparable to seawater found in the fluid inclusions of Calcite II and Calcite III suggest that these two generations of calcite are associated with seawater infiltration related to the marine transgression from 19 Ma to 15 Ma. This is also supported by the Mg enrichment in Calcite II and III (Fig. 4a, Fig. 5). Calcite IV displays an equant to *c*-axis flattened crystal morphology, which may imply that it potentially precipitated from a more dilute (fresh) groundwater (cf. Milodowski et al., 2018), and this would also be consistent with a post-Calcite IV change in groundwater chemistry. In addition, the changes of fabric in Calcite IV may possibly be explained by Oswald ripening: with the initial fine-grained or amorphous calcium carbonate precipitating rapidly with abundant nucleation sites; and subsequently, as mineralization progressed, these fine particles would have coalesced with fewer but coarser well-formed crystals growing at the expense of finer material (e.g., Dae et al., 2020).

It seems most likely that this was related to meteoric invasion following the regional uplift between 12 and 15 Ma that brought about the end of marine sedimentation. Since then, the groundwater system has been influenced by freshwater recharge both during the deposition of the lacustrine-dominated Tokai Group strata and by meteoric invasion following regional uplift up to the present day.

5.2. Source of REY in fracture-filling calcite and paleo-groundwater properties

The negative Eu anomaly and lack of significant Ce anomaly commonly observed in the REY patterns of each calcite generation are also common to both the Toki Granite and the present-day groundwater (Fig. 7; Table 2). Calcite II and Calcite III can be presumed to have precipitated from groundwater mixed with seawater, but there is no significant negative Ce anomaly and positive Eu anomaly seen in PAAS-normalized REY patterns of seawater (Deng et al., 2017). These common REY patterns in each generation of calcite indicate that the calcites precipitated from groundwater inheriting the REY pattern of the Toki

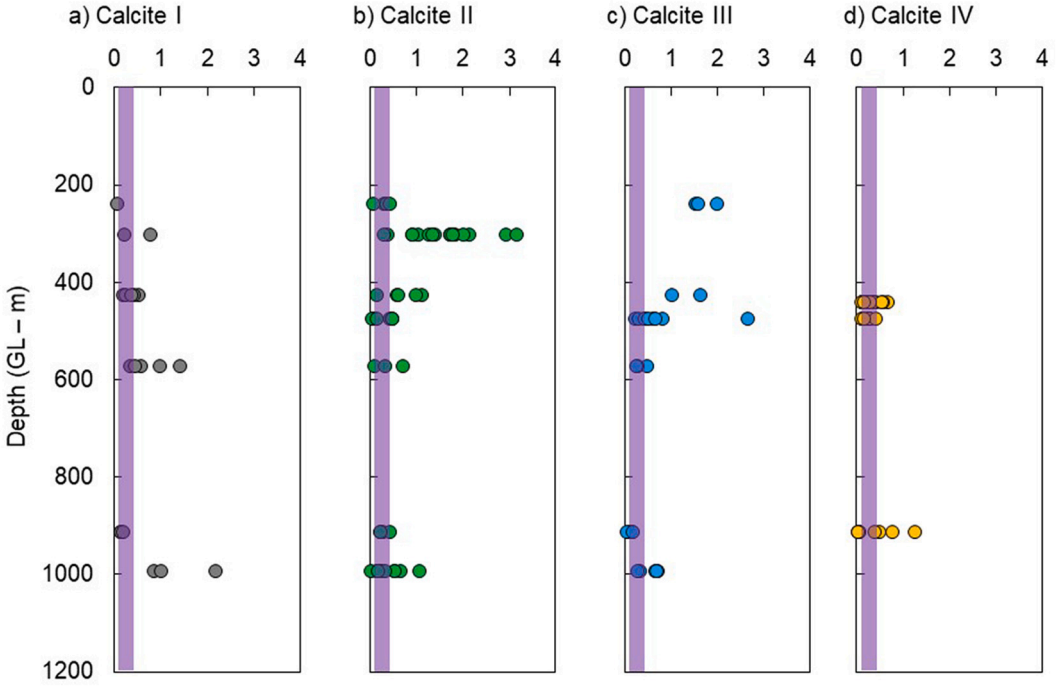

Fig. 10. Depth profile of La_{SN}/Yb_{SN} values in each generation of the calcite. The purple hatched area shows the range of the Toki granite. (For interpretation of the references to colour in this figure legend, the reader is referred to the web version of this article.)

Granite, even if groundwater is displaced by infiltration of water of different origins such as meteoric water or seawater.

Generally, Ce is removed from groundwater by precipitation as Ce (IV) in oxidizing environments (Drake et al., 2009; Marsac et al., 2017; Milodowski et al., 2018; Nakada et al., 2013). There is no evidence of a significant Ce anomaly in the fracture-filling calcites of any generation (Ce_{SN}/Ce_{SN}* 0.61–1.6, where subscript SN denotes shale (PAAS) normalization) (Table 2). The results indicate that the paleo-groundwaters remained reducing relative to the Ce (III)/Ce(IV) redox couple throughout the calcite mineralization history (Calcite I-Calcite IV). There is a good correlation between ΣREY and U concentration (r = 0.85 within all data). REY and U behave similarly in partitioning by water-rock reaction in groundwater in which carbonate complexes are predominant (Hidaka et al., 1992; McLennan and Taylor, 1979; Takahashi et al., 2002). Suzuki et al. (2016) also reported the presence of coffinite nanoparticles in fracture-filling calcite collected from the Toki Granite. They concluded that the leaching of U from the bedrock is not attributed to oxidative groundwater infiltration but increased U mobility due to complexation with dissolved carbonate. These indicate that carbonate complexes play an essential role in the long-term migration of REY and U in reducing groundwater in the Toki granite. However, there is no correlation between ΣREY and U concentration in Calcite IV, which may represent less significance of carbonate complex in the groundwater environment.

5.3. Fractionation between LREY and HREY

Studies of calcite in Swedish crystalline rocks have shown that REE fractionation patterns are related to the crystal form (Maskenskaya et al., 2015). The REY fractionation of the fracture-filling calcite investigated in this study is not related to crystal form, but the depth distribution trends are different in each generation (Fig. 10). The

Table 3
Correlation coefficient between La_{SN}/Yb_{SN} values and ΣREY, ΣLREY, and ΣHREY. Here, LREY means La, Ce, Pr, and Nd. HLEY means Er, Tm, Yb, and Lu. Gray hatched areas indicate positive or negative correlation, which shows $0.3 < |r|$ and $p < 0.05$.

		ΣREY vs La_{SN}/Yb_{SN}	ΣLREY vs La_{SN}/Yb_{SN}	ΣHREY vs La_{SN}/Yb_{SN}
Calcite I	r value	0.44	0.53	0.06
	p value	0.06	0.02	0.79
Calcite II	r value	-0.18	0.05	-0.46
	p value	0.20	0.71	0.00
Calcite III	r value	-0.31	-0.08	-0.53
	p value	0.10	0.69	0.00
Calcite IV	r value	0.36	0.59	-0.06
	p value	0.04	0.00	0.73

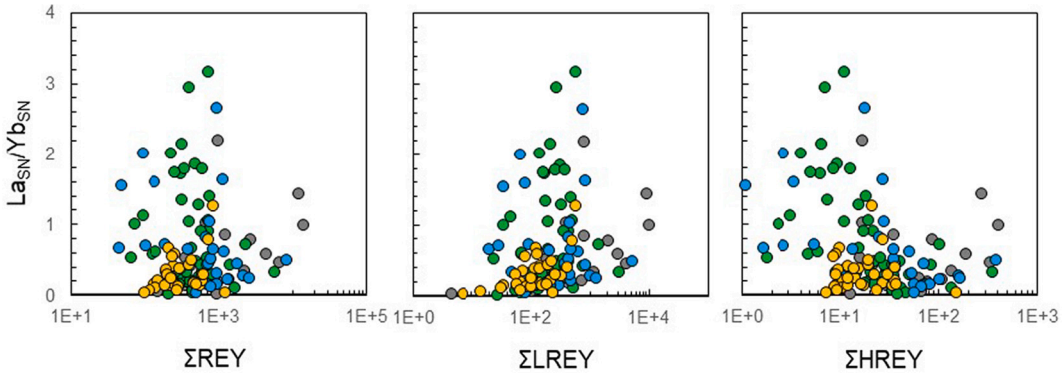

Fig. 11. Plots of La_{SN}/Yb_{SN} values vs and ΣREY, ΣLREY, and ΣHREY. The legend of each circle is the same as in Fig. 6. Here, LREY means La, Ce, Pr, and Nd. HREY means Er, Tm, Yb, and Lu. Calcite I and Calcite IV show a positive correlation with ΣLREY, and Calcite II and Calcite III show a negative correlation with ΣHREY, as shown in Table 4.

fractionation between LREY and HREY in groundwater is caused by, for example, adsorption to Fe- and Mn-hydroxides (Bau, 1999; Bau et al., 1997; Leybourne and Johannesson, 2008; Ohta and Kawabe, 2000, 2001), complexation with organic matter (Mathurin et al., 2014; Tang and Johannesson, 2005a), and adsorption and desorption with colloidal phase with changing salinity (Johannesson et al., 2017). In the present-day shallow groundwater in the Mizunami area, it was revealed that shaft excavation has led to a brief penetration by dilute surface water (Hagiwara et al., 2015), which promotes adsorption of positively charged $REYCO_3^+$ complexes dominated LREY to the bedrock, thus creating a more LREY-depleted pattern (Munemoto et al., 2015). On the other hand, the deep groundwater is not affected by such disturbances. The fractionation of LREY and HREY in each generation of calcite is discussed here, using La_{SN}/Yb_{SN} value as an indicator.

5.3.1. Calcite I

High La_{SN}/Yb_{SN} values are generally observed in the deeper part, although there is no clear correlation ($r = 0.47$, $p = 0.07$) (Fig. 10a). The change in La_{SN}/Yb_{SN} values in Calcite I depends on the change in LREY, with high La_{SN}/Yb_{SN} caused by the addition of LREY, since La_{SN}/Yb_{SN} values positively correlate with ΣLREY ($r = 0.53$) but not with ΣHREY (Table 3; Fig. 11). REY leaching tests from Toki Granite have shown the preferential leaching of LREY against HREY (Takahashi et al., 2002). Therefore, preferential LREY leaching from the Toki Granite seems to be a possible process of LREY enhancement in Calcite I.

However, normalized REY patterns in groundwaters generally tend to become enriched in HREY (e.g., Liu et al., 2016). The reason for fractionation is because lanthanide contraction results in a more significant extent of aqueous carbonate complexation for HREY relative to LREY (Lee and Byrne, 1993), leaving a greater proportion of LREY

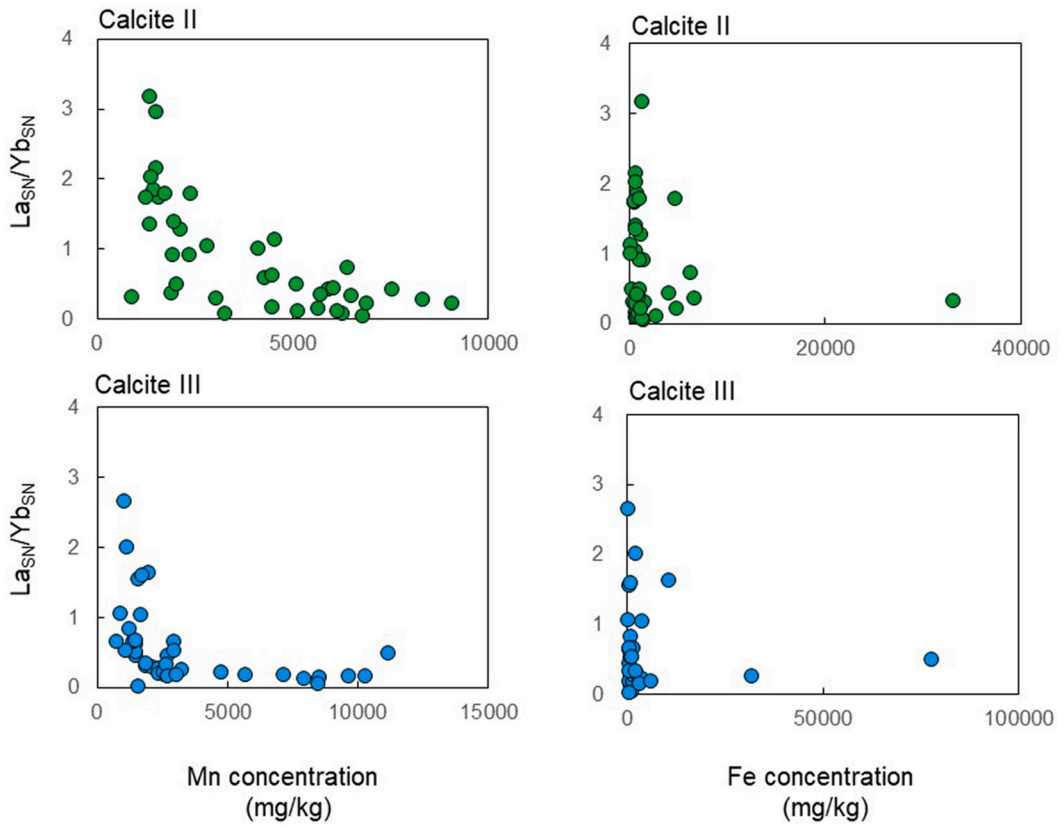

Fig. 12. La_{SN}/Yb_{SN} vs Fe and Mn plots of Calcite II and Calcite III.

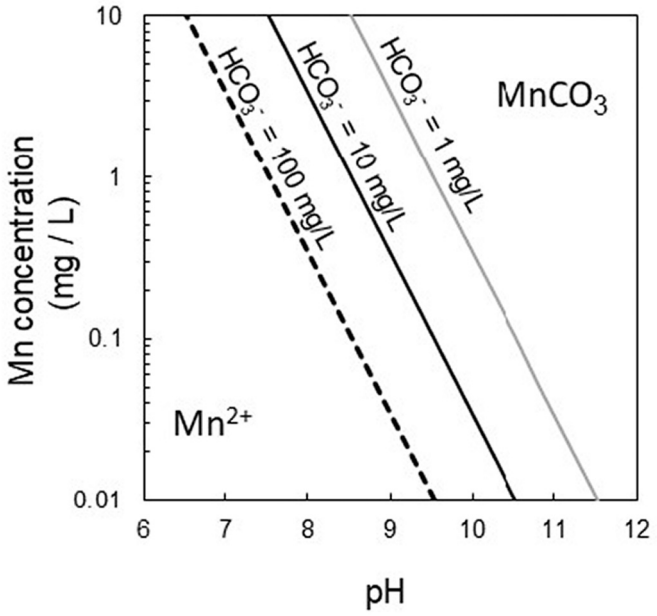

Fig. 13. Calculated result of $Mn^{2+}/MnCO_3$ reaction as a function of pH and Mn concentration.

available for adsorption onto reactive particle surfaces (Bonnand et al., 2020). Groundwater showing enrichment in LREY has been identified from the Forsmark site but is caused by LREY adsorbed on iron-rich colloids (Rönnback et al., 2008). In Calcite I, some calcite contains fragments of very finely comminuted wall rock intimately entrained and cemented within the calcite matrix, so such fragments may also have an influence on the REY abundance.

5.3.2. Calcite II and III

La_{SN}/Yb_{SN} in Calcite II and Calcite III decreased with depth ($r = -0.49$ and $r = -0.58$, respectively) (Fig. 10b, c). La_{SN}/Yb_{SN} values in Calcite II and III are negatively correlated with ΣHREY ($r = -0.46$ and $r = -0.53$, respectively) but not associated with ΣLREY (Table 3; Fig. 11). The high La_{SN}/Yb_{SN} is caused by the removal of HREY. Regarding the selective removal of HREY from REY dissolved in groundwater, Tang and Johannesson (2005b) reported that shale-normalized patterns in Canadian sandstone formations that were HREE-rich in the recharge zone became flattened as HREY were removed with groundwater flow. However, Calcite II and Calcite III show high La_{SN}/Yb_{SN} values only at the shallower part of the sequence, and no high La_{SN}/Yb_{SN} values are observed at deeper depths (Fig. 10), where the residence time of groundwater is longer. Therefore, it is unlikely that the process is associated with groundwater flow.

Mn- and Fe-hydroxides have also been shown to remove HREY (Leybourne and Johannesson, 2008; Liu et al., 2016; Mathurin et al., 2014; Tang and Johannesson, 2010). There is no correlation between Fe and La_{SN}/Yb_{SN} in Calcite II and III, but a negative correlation with Mn ($r = -0.45$ and $= -0.55$, respectively) (Fig. 12). Since Fe-hydroxide precipitation is also observed in the shallow part of the Toki granite (Iwatsuki and Yoshida, 1999), adsorption of REY on Fe-hydroxide would be expected but no evidence of this was found in this study.

In reducing carbonated groundwater, an equilibrium reaction between Mn^{2+} and $MnCO_3$ is possible (Eq. (1)), and a similar equilibrium reaction is assumed in current groundwater (Iwatsuki and Yoshida, 1999; Yamamoto et al., 2013).

$$Mn^{2+} + HCO_3^- = MnCO_3 + H^+ \quad (1)$$

Assuming an equilibrium constant of 1 (Hem, 1963) in eq. (1) and an HCO_3^- concentration of 100 mg/L, $MnCO_3$ precipitates in an alkaline environment at pH 7.5 when the Mn^{2+} concentration is 1 mg/L and at pH 8.5 or higher when the Mn concentration is 0.1 mg/L (Fig. 13). The partition coefficient of REY for $MnCO_3$ is higher in HREY (Nakada et al., 2014), causing preferential removal of HREY and Mn from groundwater. Then, the negative correlation between Mn concentration and La_{SN}/Yb_{SN} values in Calcite II and Calcite III can be considered the result of Mn and HREY removal from groundwater as precipitation of $MnCO_3$. The high La_{SN}/Yb_{SN} values are found in the shallows, indicating that the formation of $MnCO_3$ may have been enhanced by alkalization associated with the supply of HCO_3^- from the surface layer. This bicarbonate supply could have been provided by meteoric water that passed through the sedimentary rocks or by DIC in seawater related to the marine transgression.

In addition, it has also been shown that HREY preferentially forms organic complexes compared with LREY (Marsac et al., 2013; Och et al., 2014; Tang and Johannesson, 2005a). At low pH conditions (< 5), the formation of complexes between REY and organics is inhibited by major cations, such as Fe. Still, competition is minimal under near-neutral pH conditions (Marsac et al., 2013). The complexation of HREY with organics inhibits the incorporation of HREY into calcite, resulting in high La_{SN}/Yb_{SN} values. Previous studies from fractured crystalline rocks in Sweden suggested that the correlation between the concentration of organic matter in groundwater and the $\delta^{13}C$ and REY patterns in calcite indicates that the LREY-rich pattern in calcite is due to the effect of REY-organic complexes (Drake and Tullborg, 2009; Sandström and Tullborg, 2009; Tullborg et al., 1999). The bulk analysis of calcite in the shallower part of the DH-15 borehole shows low $\delta^{13}C_{PDB}$, lighter than −25‰ (Mizuno et al., 2010) (Fig. 8b), which is commonly explained by the presence of carbon having an organic origin (Sahlstedt et al., 2016; Sandström and Tullborg, 2009; Tullborg et al., 1999). The DOC concentration is mainly below the detection limit in the present-day granitic groundwater (Munemoto et al., 2015). Organic complexes are less critical than carbonate complexes in groundwater with a low concentration of organic matter (Tang and Johannesson, 2003). However, the Toki Lignite-bearing Formation is rich in organic matter (Sasao, 2013). The groundwater at that period of sedimentation of the Toki Lignite-bearing Formation is thought to have had a higher concentration of organic matter than present-day groundwater. Therefore, inhibition of coprecipitation of HREY into calcite as a result of HREY organic complex formation is a potential process of LREY enhancement in the calcite.

5.3.3. Calcite IV

In Calcite IV, La_{SN}/Yb_{SN} values and ΣLREY are positively correlated ($r = 0.59$) but not with ΣHREY (Table 3; Fig. 11). Therefore, changes in La_{SN}/Yb_{SN} values in Calcite IV, as in Calcite I, reflect changes in LREY. The depletion of LREY shown by the present-day shallow groundwater is attributed to the disturbance of underground facility construction (Munemoto et al., 2015). However, in Calcite IV, the change to groundwater of freshwater origin due to marine retreat and the recharge by dilute surface waters as a result to uplift after 1.5 Ma (Sasao et al., 2006) potentially caused LREY to be preferentially adsorbed to bedrock, resulting in a depleted LREY signature. Johannesson and Hendry (2000) investigated neutral to slightly alkaline groundwater in Canadian sedimentary rock formations. They found that $REYCO_3^+$ and $REY(CO_3)_2^-$ are the predominant dissolved chemical species for REY in shallow groundwater in LREY and HREY, respectively. The $REYCO_3^+$-dominated LREY is preferentially adsorbed by the rock, creating a depleted pattern for the LREY in the groundwater. Therefore, it indicates that preferential adsorption of LREY to bedrock can occur in shallow areas, even in the absence of artificial influences.

5.4. Y anomaly

As for the origin of the Y anomaly, it has been pointed out that Y preferentially remains in the aqueous phase due to lower complexation constants of carbonate species than the similar REYs (Ho and Er) (Möller

Table 4
Correlation coefficient between Y_{SN}/Ho_{SN} values and ΣREY, ΣLREY, and ΣHREY. Here, LREY means La, Ce, Pr, and Nd. HLEY means Er, Tm, Yb, and Lu. Gray hatched area indicate negative correlation which shows $0.3 < |r|$ and $p < 0.05$.

		ΣREY vs Y_{SN}/Ho_{SN}	ΣLREY vs Y_{SN}/Ho_{SN}	ΣHREYvs Y_{SN}/Ho_{SN}
Calcite I	r value	-0.46	-0.72	-0.35
	p value	0.04	0.00	0.13
Calcite II	r value	-0.52	-0.37	-0.71
	p value	0.00	0.01	0.00
Calcite III	r value	-0.60	-0.63	-0.58
	p value	0.00	0.00	0.00
Calcite IV	r value	-0.38	-0.38	-0.38
	p value	0.04	0.04	0.04

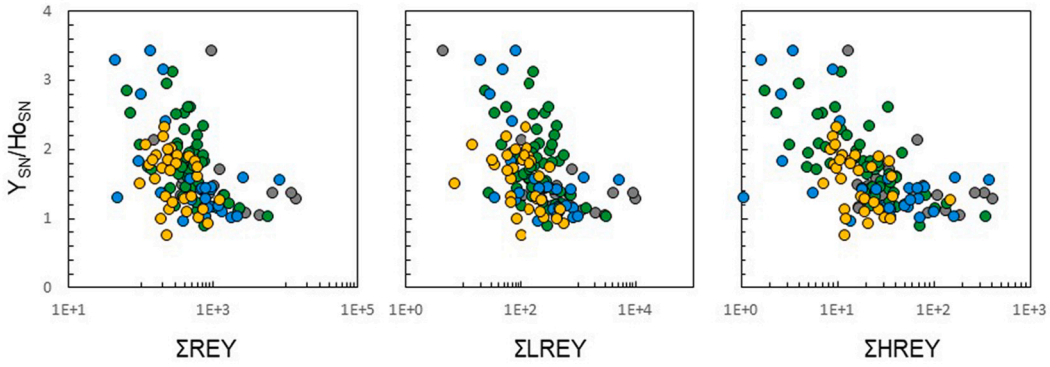

Fig. 14. Plots of Y_{SN}/Ho_{SN} values vs and ΣREY, ΣLREY, and ΣHREY. The legend of each circle is the same as in Fig. 6. All generation of calcite has a positive correlation with ΣREY, ΣLREY, and ΣHREY, except for Calcite I with ΣHREY, as shown in Table 5. Here, LREY means La, Ce, Pr, and Nd. HREY means Er, Tm, Yb, and Lu.

et al., 2021). The partition coefficient for Y is also lower for calcite than other REE (Tanaka et al., 2004). A positive Y anomaly in calcite reflects a positive Y anomaly in groundwater. Y_{SN}/Ho_{SN} in each generation of calcite is negatively correlated with both LREY and HREY, except for the relationship between Y_{SN}/Ho_{SN} values and HREY in Calcite I (Table 4; Fig. 14), indicating that the formation of Y anomaly is caused by the removal of REE except for Y.

A comparison of REY analyses of groundwater in the Toki granite that were filtered at 0.2 mm or 0.45 mm with unfiltered samples also showed a uniform decrease in all elements except Y and Eu (Munemoto et al., 2014; Takahashi et al., 2002). These results suggest that the adsorption of REY may cause the Y anomaly on suspended solids in groundwater. However, since Y_{SN}/Ho_{SN} correlate negatively with Mn only in Calcite II ($r = -0.59$), precipitation of $MnCO_3$ may be a possible adsorbed particles, as in La_{SN}/Yb_{SN}. Also, there is a positive correlation between La_{SN}/Yb_{SN} and Y_{SN}/Ho_{SN} ($r = 0.55$) in Calcite II (Fig. S1). It is also shown that Mn is present in the same fraction as La as colloids in present-day granitic groundwater (Saito et al., 2015).

6. Summary

The research focused on the interpretation of the paleohydrogeochemical evolution elucidated from mineralogical and geochemical information recorded in fracture-filling calcite mineralization in the Toki Granite in the Mizunami area. Four discrete calcite generations, from Calcite I to Calcite IV, have been differentiated based on their petrographic relationships, crystal morphological, mineral chemistry, isotopic characteristics, and chemistry of fluid inclusions. The hydrogeochemical changes in paleo-groundwaters are caused by the replacement of groundwater by seawater infiltration associated with marine transgression and by surface water infiltration associated with marine regression and uplift. Microchemical analysis of Mg, Mn, Fe, REY, and U in fracture-filling calcite also reveals a change in REY migration behavior accompanying the changes in hydrogeochemical conditions. The paragenetic sequence and the fractionation behavior of the REY in the groundwater from which calcite precipitated are also summarized in Table 5. At the time of this study, it was not possible to undertake direct age dating of the calcite samples because of limited sample size and budgetary constraints. However, in the future, if the ages of the calcite mineralization could be determined using more recent developments in laser ablation microsampling-ICP-MS U−Pb age dating techniques (e.g., Roberts et al., 2020), then it may be possible to reconstruct more detailed and better-constrained mineralization and paleo-hydrogeological history.

The PAAS-normalized REY patterns in all four generations of calcite (Calcite I – IV) show no significant Ce anomaly and a marked negative Eu anomaly. These features are also common to the Toki Granite. The consistency of the features in each generation indicates that the origin of REY in the calcite was supplied from the Toki Granite by a water-rock interaction. The lack of significant Ce anomaly in all the calcites suggests that the groundwaters were reducing throughout each generation calcite formation. The positive correlation in ΣREY and U concentrations, except Calcite IV, indicates that carbonate complex was more important species in the aqueous phase. The normalized REY patterns

Table 5
The paragenetic sequence of calcite mineralization and estimated REY behavior in granitic groundwater and its potential correlation with key geological events (from Sasao et al., 2006; Yamasaki and Umeda, 2012) in the Mizunami area.

Timescale	Geological event	Origin of groundwaters in the basement granite	Calcite generation	Estimated REY behavior in fracture-filling calcite
c.75 Ma	Toki Granite intrusion			
37.6–39.8 Ma	Late-stage cooling of the granite	Warm hydrothermal fluid [90 °C to 120 °C]	Calcite I	Intense water-rock interaction induces LREY-enrichment in the groundwater and calcite
37.6–27 Ma	uplift and subareal exposure and erosion (Deep weathering of Toki granite)	Meteoric [Freshwater]		
27–20 Ma?	Deposition of the Toki Lignite-bearing Fm	Meteoric + Riverine [Freshwater]		Removal of HREY from groundwater associated with precipitation of $MnCO_3$ and/or adsorption on organic matters in shallow area cause LREY enhancement in the calcite
19–18 Ma?	Deposition of the Hongo Formation	Seawater invasion [Saline]	Calcite II & Calcite III	
c.17 Ma	Deposition of Akeyo Formation			
17–15 Ma	Unconformity	Possible meteoric invasion? [?Freshwater]		
c. 15 Ma	Deposition of the Oidawara Formation	Seawater invasion [Saline]		
15–12 Ma	Major unconformity between Mizunami and Tokai Group	Meteoric invasion [Freshwater]		
12–1.5 Ma	Deposition of the Tokai Group sediments	Meteoric + Lacustrine] [Freshwater recharge]		Removal of LREY from groundwater associated with adsorption on bedrock cause HREY enhancement in the calcite
c. 1.5-present	Base-level change due to regional uplift	Meteoric invasion ongoing [Freshwater recharge]	Calcite IV	

for Calcite I, II, and III generally show an enhancement in LREY relative to HREY compared to that seen in the granite host rock. In contrast, the normalized REY patterns for Calcite IV show less enhancement of LREY, more closely reflecting the REY distribution of the granite. The study results on REY fractionation in the calcite based on La_{SN}/Yb_{SN} and Y_{SN}/Ho_{SN} revealed the following processes. Calcite I in the deeper part shows a LREY-enrichment pattern, which is caused by the preferential release of LREY by water-rock interaction and/or influence of wall rock fragments which preferentially adsorbed LREY. Calcites II and Calcite III show high La_{SN}/Yb_{SN} in the shallow part, which is induced by coprecipitation of HREY with $MnCO_3$ or selective adsorption of HREY on organic matter in paleo-groundwater. Calcite IV shows more LREY depleted patterns caused by adsorption of LREY on bedrock. In addition, the positive Y anomaly identified in the calcite reflects the low formation constant of Y with carbonic species. It is inferred to be due to the adsorption of REE other than Y on suspended particles in groundwaters.

These variations of REY behavior are closely related to changes in the carbonate concentration and/or pH in palaeo-groundwater, and REY carbonate speciation, indicating that understanding them is essential for understanding the long-term REY behavior in groundwater. The findings of this study will be necessary for assessing the long-term safety of geological disposal of HLRW.

Declaration of Competing Interest

The authors declare that they have no known competing financial interests or personal relationships that could have appeared to influence the work reported in this paper.

Acknowledgments

The authors thank S. Chenery (BGS) and J. Bouch (BGS) for their support in the provision of LAMP-ICPMS and EMPA analyses of the calcite samples. AEM publishes with the permission of the Director of the British Geological Survey, part of United Kingdom Research and Innovation (UKRI). We also thank K. Hama (JAEA) and H. Sasamoto (JAEA) for improving the manuscript. Editorial work by K. H. Johannesson and thoughtful and constructive comments by M. I. Leybourne and K. H. Johannesson, and two anonymous reviewers improved the manuscript.

Appendix A. Supplementary data

Supplementary data to this article can be found online at https://doi.org/10.1016/j.chemgeo.2022.120880.

References

Astilleros M, J, Pina M, C, Ferna´ndez-Dı´az, L, Putnis, A, 2002. Molecular-scale surface processes during the growth of calcite in the presence of manganese. Geochimica et Cosmochimica Acta 66 (18), 3177–3189.
Barnaby, R.J., Rimstidt, J.D., 1989. Redox conditions of calcite cementation interpreted from Mn and Fe contents of authigenic calcites. GSA Bull. 101, 795–804.
Bau, M., 1999. Scavenging of dissolved yttrium and rare earths by precipitating iron oxyhydroxide: Experimental evidence for Ce oxidation, Y-Ho fractionation, and lanthanide tetrad effect. Geochim. Cosmochim. Acta 63, 67–77. https://doi.org/10.1016/S0016-7037(99)00014-9.
Bau, M., Möller, P., Dulski, P., 1997. Yttrium and lanthanides in eastern Mediterranean seawater and their fractionation during redox-cycling. Mar. Chem. 56, 123–131. https://doi.org/10.1016/S0304-4203(96)00091-6.
Blyth, A.R., Frape, S.K., Tullborg, E.L., 2009. A review and comparison of fracture mineral investigations and their application to radioactive waste disposal. Appl. Geochem. 24, 821–835. https://doi.org/10.1016/j.apgeochem.2008.12.036.
Bonnand, P., Lalonde, S.V., Boyet, M., Heubeck, C., Homann, M., Nonnotte, P., Foster, I., Konhauser, K.O., Köhler, I., 2020. Post-depositional REE mobility in a Paleoarchean banded iron formation revealed by La-Ce geochronology: a cautionary tale for signals of ancient oxygenation. Earth Planet. Sci. Lett. 547, 116452 https://doi.org/10.1016/j.epsl.2020.116452.
Chenery, S., Cook, J.M., 1993. Determination of Rare Earth Element in single mineral grains by laser ablation microprobe-inductively coupled plasma mass spectrometry. J. Anal. At. Spectrom. 8, 299–303.
Dae, K.S., Chang, J.H., Koo, K., Park, J., Kim, J.S., Yuk, J.M., 2020. Real-Time Observation of CaCO3Mineralization in Highly Supersaturated Graphene Liquid Cells. ACS Omega 5, 14619–14624. https://doi.org/10.1021/acsomega.0c01300.
Davis, K.J., Dove, P.M., Wasylenki, L.E., De Yoreo, J.J., 2004. Morphological consequences of differential Mg2+ incorporation at structurally distinct steps on calcite. Am. Mineral. 89, 714–720.
Deng, Y., Ren, J., Guo, Q., Cao, J., Wang, H., Liu, C., 2017. Rare earth element geochemistry characteristics of seawater and porewater from deep sea in western Pacific. Sci. Rep. 7, 1–13. https://doi.org/10.1038/s41598-017-16379-1.
Drake, H., Tullborg, E., 2009. Paleohydrogeological events recorded by stable isotopes, fluid inclusions and trace elements in fracture minerals in crystalline rock, Simpevarp area. SE Sweden. Appl. Geochem. 24, 715–732. https://doi.org/10.1016/j.apgeochem.2008.12.026.
Drake, H., Tullborg, E., Mackenzie, A.B., 2009. Detecting the near-surface redox front in crystalline bedrock using fracture mineral distribution, geochemistry and U-series disequilibrium. Appl. Geochem. 24, 1023–1039. https://doi.org/10.1016/j.apgeochem.2009.03.004.
Emrich, K., Ehhalt, D.H., Vogel, J.C., 1970. Carbon isotope fractionation during the precipitation of calcium carbonate. Earth Planet. Sci. Lett. 8, 363–371.
Folk, R.L., 1974. The natural history of crystalline calcium carbonate: effect of magnesium content and salinity. SEPM J. Sediment. Res. 44, 40–53. https://doi.org/10.1306/74d72973-2b21-11d7-8648000102c1865d.

Frank, J.R., Carpenter, A.B., Oglesby, T.W., 1982. Cathodoluminescence and composition of calcite cement in the Taum Sauk Limestone (Upper Cambrian), Southeast Missouri. J. Sediment. Res. 52, 631–638.
Franklyn, M.T., McNutt, R.H., Kamineni, D.C., Gascoyne, M., Frape, S.K., 1991. Groundwater 87Sr/86Sr values in the Eye-Dashwa Lakes pluton, Canada: evidence for plagioclase-water reaction. Chem. Geol. Isot. Geosci. Sect. 86, 111–122. https://doi.org/10.1016/0168-9622(91)90057-4.
Given, R.K., Wilkinson, B.H., 1985. Kinetic control of morphology, composition, and mineralogy of abiotic sedimentary carbonates. J. Sediment. Res. 55, 109–119.
Gonzalez, L.A., Carpenter, S.J., Lohmann, K.C., 1992. Inorganic calcite morphology; roles of fluid chemistry and fluid flow. J. Sediment. Res. 62, 382–399.
Hagiwara, H., Iwatsuki, T., Hasegawa, T., Nakata, K., Tomioka, Y., 2015. Shallow groundwater intrusion to deeper depths caused by construction and drainage of a large underground facility. J. Japanese Assoc. Hydrol. Sci. 45, 21–38. https://doi.org/10.4145/jahs.45.21.
Hem, J., 1963. Chemical equilibria and rates of manganese oxidation - Chemistry of Manganese in Natural Water. US Geol. Surv. Water-Supply Pap. 1667-A 71.
Hidaka, H., Masuda, A., Shimizu, H., Holliger, P., 1992. Lanthanide tetrad effect observed in the Oklo and ordinary uraninites and its implication for their forming processes. Geochem. J. 26, 337–346. https://doi.org/10.2343/geochemj.26.337.
Hiroki, Y., Matsumoto, R., 1999. Magnetostratigraphic correlation of Miocene regression-and-transgression boundaries in central Japan. J. Geol. Soc. Japan 105, 81–107. https://doi.org/10.1248/cpb.37.3229.
Ishibashi, M., Yoshida, H., Sasao, E., Yuguchi, T., 2016. Long term behavior of hydrogeological structures associated with faulting: an example from the deep crystalline rock in the Mizunami URL, Central Japan. Eng. Geol. 208, 114–127. https://doi.org/10.1016/j.enggeo.2016.04.026.
Iwatsuki, T., Yoshida, H., 1999. Groundwater chemistry and fracture mineralogy in the basement granitic rock in the Tono uranium mine area, Gifu Prefecture, Japan—Groundwater composition, Eh evolution analysis by fracture filling mineral—. Geochem. J. 33.
Iwatsuki, Teruki, Munemoto, Takashi, Kubota, Mitsuru, Hayashida, Kazuki, Kato, Toshihiro, 2017. Characterization of rare earth elements (REEs) associated with suspended particles in deep granitic groundwater and their post-closure behavior from a simulated underground facility. Appl. Geochem. J. 82, 134–145. https://doi.org/10.1016/j.apgeochem.2017.04.016.
Iwatsuki, T., Satake, H., Metcalfe, R., Yoshida, H., Hama, K., 2002. Isotopic and morphological features of fracture calcite from granitic rocks of the Tono area, Japan : a promising palaeohydrogeological tool. Appl. Geochem. 17, 1241–1257.
Iwatsuki, T., Furue, R., Mie, H., Ioka, S., Mizuno, T., 2005. Hydrochemical baseline condition of groundwater at the Mizunami underground research laboratory (MIU). Appl. Geochem. 20, 2283–2302. https://doi.org/10.1016/j.apgeochem.2005.09.002.
Iwatsuki, T., Mizuno, T., Hama, K., Kunimaru, T., 2010. Mineralogical analysis of a long-term groundwater system in Tono and Horonobe area, Japan. In: Taniguchi, M., Holman, I.P. (Eds.), Groundwater Response to Changing Climate. CRC Press, pp. 87–98.
JAEA, 2011. Final Report on the Surface-Based Investigation Phase (Phase I)at the Mizunami UndergroundResearch Laboratory Project.
JAEA, 2016. Synthesized research report in the second mid-term research phase - mizunami underground research laboratory project, horonobe underground research laboratory project and geo-stability project. JAEA-Review 2016-014. https://doi.org/10.11484/jaea-review-2016-014.
JNC, 2000. Regional Hydrogeological Study Project Results from 1992–1999 (Revised Edition).
Johannesson, K.H., Hendry, M.J., 2000. Rare earth element geochemistry of groundwaters from a thick till and clay-rich aquitard sequence, Saskatchewan, Canada. Geochim. Cosmochim. Acta 64, 1493–1509. https://doi.org/10.1016/S0016-7037(99)00402-0.
Johannesson, K.H., Palmore, C.D., Fackrell, J., Prouty, N.G., Swarzenski, P.W., Chevis, D. A., Telfeyan, K., White, C.D., Burdige, D.J., 2017. Rare earth element behavior during groundwater–seawater mixing along the Kona Coast of Hawaii. Geochim. Cosmochim. Acta 198, 229–258. https://doi.org/10.1016/j.gca.2016.11.009.
Kimbell, T, Humphrey, J, 1994. Geochemistry and crystal morphology of aragonite cements of mixing-zone origin, Barbados, West Indies. Journal of Sedimentary Research 64 (3a), 604–614.
Lahann, R.W., 1978. A chemical model for calcite crystal growth and morphology control. J. Sediment. Res. 48, 337–347.
Lee, J.H., Byrne, R.H., 1993. Complexation of trivalent rare earth elements (Ce, Eu, Gd, Tb, Yb) by carbonate ions. Geochim. Cosmochim. Acta 57, 295–302. https://doi.org/10.1016/0016-7037(93)90432-V.
Leybourne, M.I., Johannesson, K.H., 2008. Rare earth elements (REE) and yttrium in stream waters, stream sediments, and Fe-Mn oxyhydroxides: Fractionation, speciation, and controls over REE + Y patterns in the surface environment. Geochim. Cosmochim. Acta 72, 5962–5983. https://doi.org/10.1016/j.gca.2008.09.022.
Liu, H., Guo, H., Xing, L., Zhan, Y., Li, F., Shao, J., Niu, H., Liang, X., Li, C., 2016. Geochemical behaviors of rare earth elements in groundwater along a flow path in the North China Plain. J. Asian Earth Sci. 117, 33–51. https://doi.org/10.1016/j.jseaes.2015.11.021.
Marsac, R., Davranche, M., Gruau, G., Dia, A., Pédrot, M., Le Coz-Bouhnik, M., Briant, N., 2013. Effects of Fe competition on REE binding to humic acid: origin of REE pattern variability in organic waters. Chem. Geol. 342, 119–127. https://doi.org/10.1016/j.chemgeo.2013.01.020.
Marsac, R., Réal, F., Banik, N.L., Pédrot, M., Pourret, O., Vallet, V., 2017. Aqueous chemistry of Ce(IV): Estimations using actinide analogues. Dalton Trans. 46, 13553–13561. https://doi.org/10.1039/c7dt02251d.
Maskenskaya, O.M., Drake, H., Mathurin, F.A., Åström, M.E., 2015. The role of carbonate complexes and crystal habit on rare earth element uptake in low-temperature calcite in fractured crystalline rock. Chem. Geol. 391, 100–110. https://doi.org/10.1016/j.chemgeo.2014.10.030.
Mathurin, F.A., Åström, M.E., Drake, H., Maskenskaya, O.M., Kalinowski, B.E., 2014. REE and Y in groundwater in the upper 1.2km of Proterozoic granitoids (Eastern Sweden) - assessing the role of composition and origin of groundwaters, geochemistry of fractures, and organic/inorganic aqueous complexation. Geochim. Cosmochim. Acta 144, 342–378. https://doi.org/10.1016/j.gca.2014.08.004.
McLennan, M.S., Taylor, S.R., 1979. Rare earth element mobility associated with uranium mineralisation. Nature 282, 247–250.
Metcalfe, R., Hooker, P., Darling, W.G., Milodowski, A.E., 1998. Dating Quaternary groundwater flow events: a review of avail-able methods and their application. In: Parnell, J. (Ed.), Dating and Duration of Fluid Flow and Fluid Rock Interaction. Geological Society of London Special Publication, pp. 233–260.
Metcalfe, R., Hama, K., Amano, K., Iwatsuki, T., Saegusa, H., 2003. Geochemical approaches to understanding a deep groundwater flow system in the Tono area, Gifu-ken, Japan. In: Groundwater Engineering - Recent Advances, pp. 555–562. https://doi.org/10.1201/9781439833605.ch73.
Miekeley, N., Coutinho de Jesus, H., Porto da Silveira, C.L., Degueldre, C., 1992. Chemical and physical characterization of suspended particles and colloids in waters from the Osamu Utsumi mine and Morro do Ferro analogue study sites, Poços de Caldas, Brazil. J. Geochem. Explor. 45, 409–437. https://doi.org/10.1016/0375-6742(92)90133-S.
Milodowski, A.E., Gillespie, M.R., Naden, J., Fortey, N.J., Shepherd, T.J., Pearce, J.M., Metcalfe, R., 1998. The petrology and paragenesis of fracture mineralization in the Sellafield area, west Cumbria. Proc. Yorks. Geol. Soc. 52, 215–241.
Milodowski, A.E., Tullborg, E.-L., Buil, B., Gómez, P., Turrero, M.J., Haszeldine, S.G.E., Gillespie, M.R., Torres, T., Ortiz, J.E., Zachariáš, J., Šilar, J., ALM, Chvátal, Strnad, L., Šebek, O., Bouch, J.E., Chenery, S.R., Chenery, C., Shepherd, T.J., McKervey, J.A., 2005. Application of Mineralogical, Petrological and Geochemical Tools for Evaluating the Palaeohydrogeological Evolution of the PADAMOT Study Sites.
Milodowski, A.E., Alexander, W.R., West, J.M., Shaw, R.P., McEvoy, F.M., Scheidegger, J.M., Field, L.P., 2015. A catalogue of analogues for radioactive waste management. Br. Geol. Surv. 1–184.
Milodowski, A.E., Bath, A., Norris, S., 2018. Palaeohydrogeology using geochemical, isotopic and mineralogical analyses: Salinity and redox evolution in a deep groundwater system through Quaternary glacial cycles. Appl. Geochem. 97, 40–60. https://doi.org/10.1016/j.apgeochem.2018.07.008.
Mizuno, T., Milodowski, A.E., Iwatsuki, T., 2010. Evaluation of the long-term evolution of the groundwater system in the Mizunami Area, Japan. In: ASME 2010 13th International Conference on Environmental Remediation and Radioactive Waste Management, Vol. 2. ASME, pp. 193–201. https://doi.org/10.1115/ICEM2010-40070.
Möller, P., De Lucia, M., 2020. Incorporation of rare earths and yttrium in calcite: a critical re-evaluation. Aquat. Geochem. 26, 89–117. https://doi.org/10.1007/s10498-020-09369-9.
Möller, P., Dulski, P., De Lucia, M., 2021. REY patterns and their natural anomalies in waters and brines: the correlation of Gd and Y anomalies. Hydrology 8. https://doi.org/10.3390/hydrology8030116.
Munemoto, T., Ohmori, K., Iwatsuki, T., 2014. Distribution of U and REE on colloids in granitic groundwater and quality-controlled sampling at the Mizunami underground research laboratory. Prog. Earth Planet. Sci. 1 https://doi.org/10.1186/s40645-014-0028-z.
Munemoto, T., Ohmori, K., Iwatsuki, T., 2015. Rare earth elements (REE) in deep groundwater from granite and fracture-filling calcite in the Tono area, Central Japan: prediction of REE fractionation in paleo- to present-day groundwater. Chem. Geol. 417, 58–67. https://doi.org/10.1016/j.chemgeo.2015.09.024.
Nakada, R., Takahashi, Y., Tanimizu, M., 2013. Isotopic and speciation study on cerium during its solid-water distribution with implication for Ce stable isotope as a paleo-redox proxy. Geochim. Cosmochim. Acta 103, 49–62. https://doi.org/10.1016/j.gca.2012.10.045.
Nakada, R., Shirai, T., Takahashi, S., Suzuki, N., Ogawa, K., Takahashi, Y., 2014. A geochemical constraint on the formation process of a manganese carbonate nodule in the siliceous mudstone of the Jurassic accretionary complex in the Mino Belt, Japan. J. Asian Earth Sci. 96, 59–68. https://doi.org/10.1016/j.jseaes.2014.08.032.
Och, L.M., Müller, B., Wichser, A., Ulrich, A., Vologina, E.G., Sturm, M., 2014. Rare earth elements in the sediments of Lake Baikal. Chem. Geol. 376, 61–75. https://doi.org/10.1016/j.chemgeo.2014.03.018.
OECD NEA, 2013. The Nature and Purpose of the Post-Closure Safety Cases for Geological Repositories.
OECD/NEA, 2012. Methods for Safety Assessment of Geological Disposal Facilities for Radioactive Waste Radioactive Waste Management 2012.
Ohta, A., Kawabe, I., 2000. Rare eath element partitioning between fe oxyhydroxide precipitates and aqueous NaCl solutions doped with NaHCO3: Determinations of rare earth element complexation constants with carbonate ions. Geochem. J. 34, 439–454. https://doi.org/10.2343/geochemj.34.439.
Ohta, A., Kawabe, I., 2001. REE(III) adsorption onto Mn dioxide (δ-Mn02) and Fe oxyhydroxide: Ce(III) oxidation by δ-MnO2. Geochim. Cosmochim. Acta 65, 695–703. https://doi.org/10.1016/S0016-7037(00)00578-0.
O'Neil, J.R., Clayton, R.N., Mayeda, T.K., 1969. Oxygen isotope fractionation in divalent metal carbonates. J. Chem. Phys. 51, 5547–5558. https://doi.org/10.1063/1.1671982.

Parker, S.C., Titiloye, J.O., Watson, G.W., 1993. Molecular modelling of carbonate minerals: studies of growth and morphology. Philosophical Transactions of the Royal Society A 344 (1670), 37–48. https://doi.org/10.1098/rsta.1993.0073.

Pourmand, A., Dauphas, N., Ireland, T.J., 2012. A novel extraction chromatography and MC-ICP-MS technique for rapid analysis of REE, Sc and Y: revising CI-chondrite and Post-Archean Australian Shale (PAAS) abundances. Chem. Geol. 291, 38–54. https://doi.org/10.1016/j.chemgeo.2011.08.011.

Qin, H.B., Yang, S., Tanaka, M., Sanematsu, K., Arcilla, C., Takahashi, Y., 2020. Chemical speciation of scandium and yttrium in laterites: New insights into the control of their partitioning behaviors. Chem. Geol. 552, 119771 https://doi.org/10.1016/j.chemgeo.2020.119771.

Roberts, N.M.W., Drost, K., Horstwood, M.S.A., Condon, D.J., Chew, D., Drake, H., Milodowski, A.E., McLean, N.M., Smye, A.J., Walker, R.J., Haslam, R., Hodson, K., Imber, J., Beaudoin, N., Lee, J.K., 2020. Laser ablation inductively coupled plasma mass spectrometry (LA-ICP-MS) U–Pb carbonate geochronology: strategies, progress, and limitations. Geochronology 2, 33–61. https://doi.org/10.5194/gchron-2-33-2020.

Roedder, E., 1984. In: Reviews in. (Ed.), Fluid Inclusions. Mineralogical Society of America, Washington D.C.

Rönnback, P., Åström, M., Gustafsson, J.P., 2008. Comparison of the behaviour of rare earth elements in surface waters, overburden groundwaters and bedrock groundwaters in two granitoidic settings, Eastern Sweden. Appl. Geochem. 23, 1862–1880. https://doi.org/10.1016/j.apgeochem.2008.02.008.

Sahlstedt, E., Karhu, J.A., Pitkänen, P., Whitehouse, M., 2016. Biogenic processes in crystalline bedrock fractures indicated by carbon isotope signatures of secondary calcite. Appl. Geochem. 67, 30–41. https://doi.org/10.1016/j.apgeochem.2016.01.010.

Saito, T., Hamamoto, T., Mizuno, T., Iwatsuki, T., Tanaka, S., 2015. Comparative study of granitic and sedimentary groundwater colloids by flow-field flow fractionation coupled with ICP-MS. J. Anal. At. Spectrom. 30, 1229–1236. https://doi.org/10.1039/C5JA00088B.

Sakamaki, Y., 1985. Geologic environments of Ningyo-toge and Tono uranium deposits, Japan, IAEA-TECDO. ed, Geological Environments of Sandstone-Type Uranium Deposits. IAEA.

Sandström, B., Tullborg, E., 2009. Episodic fluid migration in the Fennoscandian Shield recorded by stable isotopes, rare earth elements and fluid inclusions in fracture minerals at Forsmark, Sweden. Chem. Geol. https://doi.org/10.1016/j.chemgeo.2009.04.019.

Sasao, E., 2013. Petrographic study of the Miocene Mizunami Group, Central Japan: detection of unrecognized volcanic activity in the Setouchi Province. Island Arc 22, 170–184. https://doi.org/10.1111/iar.12019.

Sasao, E., Ota, K., Iwatsuki, T., Niizato, T., Arthur, R.C., Stenhouse, M.J., Zhou, W., Metcalfe, R., Takase, H., Mackenzie, A.B., 2006. An overview of a natural analogue study of the Tono Uranium Deposit, central Japan. Geochem. Explor. Environ. Anal. https://doi.org/10.1144/1467-7873/05-084.

Stipp, S.L.S., Christensen, J.T., Lakshtanov, L.Z., Baker, J.A., Waight, T.E., 2006. Rare Earth element (REE) incorporation in natural calcite: Upper limits for actinide uptake in a secondary phase. Radiochim. Acta 94, 523–528. https://doi.org/10.1524/ract.2006.94.9-11.523.

Suzuki, Y., Konno, U., Fukuda, A., Komatsu, D.D., Hirota, A., Watanabe, K., Togo, Y., Morikawa, N., Hagiwara, H., Aosai, D., Iwatsuki, T., Tsunogai, U., Nagao, S., Ito, K., Mizuno, T., 2014. Biogeochemical signals from deep microbial life in terrestrial crust. PLoS One 9, e113063. https://doi.org/10.1371/journal.pone.0113063.

Suzuki, Y., Mukai, H., Ishimura, T., Yokoyama, T.D., Sakata, S., Hirata, T., Iwatsuki, T., Mizuno, T., 2016. Formation and geological sequestration of uranium nanoparticles in deep granitic aquifer. Sci. Rep. 6, 22701. https://doi.org/10.1038/srep22701.

Takahashi, Y., Yoshida, H., Sato, N., Hama, K., Yusa, Y., Shimizu, H., 2002. W- and M-type tetrad effects in REE patterns for water-rock systems in the Tono uranium deposit, Central Japan. Chem. Geol. 184, 311–335. https://doi.org/10.1016/S0009-2541(01)00388-6.

Takeuchi, S., Saegusa, H., Amano, K., Takeuchi, R., 2013. Hydrogeological characterization of deep subsurface structures at the Mizunami Underground Research Laboratory. J. Geol. Soc. Japan 119, 75–90. https://doi.org/10.5575/geosoc.2011.0013.

Tanaka, K., Kawabe, I., 2006. REE abundances in ancient seawater inferred from marine limestone and experimental REE partition coefficients between calcite and aqueous solution. Geochem. J. 40, 425–435. https://doi.org/10.2343/geochemj.40.425.

Tanaka, K., Ohta, A., Kawabe, I., 2004. Experimental REE partitioning between calcite and aqueous solution at 25°C and 1 atm: constraints on the incorporation of seawater REE into semount-type limestones. Geochem. J. 38, 19–32. https://doi.org/10.2343/geochemj.38.19.

Tang, J., Johannesson, K.H., 2003. Speciation of rare earth elements in natural terrestrial waters: assessing the role of dissolved organic matter from the modeling approach. Geochim. Cosmochim. Acta 67, 2321–2339. https://doi.org/10.1016/S0016-7037(02)01413-8.

Tang, J., Johannesson, K.H., 2005a. Adsorption of rare earth elements onto Carrizo sand: experimental investigations and modeling with surface complexation. Geochim. Cosmochim. Acta 69, 5247–5261. https://doi.org/10.1016/j.gca.2005.06.021.

Tang, J., Johannesson, K.H., 2005b. Rare earth element concentrations, speciation, and fractionation along groundwater flow paths: the Carrizo Sand (Texas) and Upper Floridan aquifers. In: Rare Earth Elements in Groundwater Flow Systems, pp. 223–244.

Tang, J., Johannesson, K.H., 2010. Ligand extraction of rare earth elements from aquifer sediments: Implications for rare earth element complexation with organic matter in natural waters. Geochim. Cosmochim. Acta 74, 6690–6705. https://doi.org/10.1016/j.gca.2010.08.028.

Temmam, M., Paquette, J., Vali, H., 2000. Mn and Zn incorporation into calcite as a function of chloride aqueous concentration. Geochim. Cosmochim. Acta 64 (14), 2417–2430.

Terakado, Y., Masuda, A., 1988. The coprecipitation of rare-earth elements with calcite and aragonite. Chem. Geol. 69, 103–110. https://doi.org/10.1016/0009-2541(88)90162-3.

Toyama, K., Terakado, Y., 2014. Experimental study of rare earth element partitioning between calcite and sodium chloride solution at room temperature and pressure. Geochem. J. 48, 463–477. https://doi.org/10.2343/geochemj.2.0322.

Tullborg, E., Drake, H., 2008. Palaeohydrogeology : a methodology based on fracture mineral studies. Appl. Geochem. 23, 1881–1897. https://doi.org/10.1016/j.apgeochem.2008.02.009.

Tullborg, E.-L., Landström, O., Wallin, B., 1999. Low-temperature trace element mobility influenced by microbial activity—indications from fracture calcite and pyrite in crystalline basement. Chem. Geol. 157, 199–218. https://doi.org/10.1016/S0009-2541(99)00002-9.

Voigt, M., Mavromatis, V., Oelkers, E.H., 2017. The experimental determination of REE partition coefficients in the water-calcite system. Chem. Geol. 462, 30–43. https://doi.org/10.1016/j.chemgeo.2017.04.024.

Wogelius, R.A., Milodowski, A.E., Field, L.P., Metcalfe, R., Lowe, T., van Veelen, A., Carpenter, G., Norris, S., Yardley, B., 2020. Mineral reaction kinetics constrain the length scale of rock matrix diffusion. Sci. Rep. 10 https://doi.org/10.1038/s41598-020-65113-x.

Wood, S.A., 1990. The aqueous geochemistry of the rare-earth elements and yttrium. 1. Review of available low-temperature data for inorganic complexes and the inorganic REE speciation of natural waters. Chem. Geol. 82, 159–186. https://doi.org/10.1016/0009-2541(90)90080-Q.

Yamamoto, K., Yoshida, H., Akagawa, F., Nishimoto, S., Metcalfe, R., 2013. Redox front penetration in the fractured Toki Granite, Central Japan: an analogue for redox reactions and redox buffering in fractured crystalline host rocks for repositories of long-lived radioactive waste. Appl. Geochem. 35, 75–87. https://doi.org/10.1016/j.apgeochem.2013.03.013.

Yamasaki, S., Umeda, K., 2012. Cooling history of the CretaceousTokigranite in theeastern Sanyo Belt, Central Japan. Japanese Mag. Mineral. Petrol. Sci. 41, 39–46. https://doi.org/10.2465/gkk.101203.

Zhong, S., Mucci, A., 1995. Partitioning of rare earth elements (REEs) between calcite and seawater solutions at 25°C and 1 atm, and high dissolved REE concentrations. Geochim. Cosmochim. Acta 59, 443–453. https://doi.org/10.1016/0016-7037(94)00381-U.